Innate Antifungal Immune Receptor, Dectin-1, Undergoes Ligand-Induced Oligomerization with Highly Structured β-Glucans and at Fungal Cell Contact Sites

Authors:

Eduardo U. Anaya[1], Akram Etemadi Amin[1,2], Mike Danielson[3], Kyle Michel[3], Aaron K. Neumann[1,4]

Affiliations:

1. Department of Pathology, University of New Mexico, School of Medicine, Albuquerque, NM, USA, 87131

2. Department of Physics and Astronomy, University of New Mexico, Albuquerque, NM, USA 87131

3. ImmunoResearch Inc., Eagan, MN, USA, 55121

4. Corresponding author: akneumann@salud.unm.edu

Keywords:

Dectin-1, dimer, beta-glucan, *Candida albicans*, hemITAM, Syk, Calcium signaling, FRET, RICS, N&B

Author Summary

Candidemia is the most common bloodstream infection in the United States. During infection, the fungal cell wall is an important virulence factor, playing roles in adhesion, immune recognition and colonization. The human innate immune system recognizes β-glucan, a highly immunogenic component of the fungal cell wall. During innate immune recognition of *Candida*, the organization of cell wall β-glucan is an important determinant of a successful immune activation. However, there have been many reports showing conflicting biological activities of β-glucans with different size, branching and structure. Here, using quantitative fluorescence imaging techniques, we investigate how differential size and structure of β-glucan impacts activation of the innate immune receptor, Dectin-1A. Our results indicate a positive correlation between highly structured glucans and Dectin-1A activation. Furthermore, we determined this is due to the higher ordered β-glucan causing Dectin-1A receptors to form aggregates that are below 15 nm in size. Finally, Dectin-1A receptor aggregation has also been shown to form at fungal particle contact sites with high β-glucan exposure.

Abstract

Dectin-1A is a C-type Lectin innate immunoreceptor that recognizes β-(1,3:1,6)-glucan, a structural component of *Candida* species cell walls. The higher order structure of β-glucans ranges from random coil to insoluble fiber due to varying degrees of tertiary (helical) and quaternary structure. Model *Saccharomyces cerevisiae* β-glucans of medium and high molecular weight (MMW and HMW, respectively) are highly structured. In contrast, low MW glucan (LMW) is much less structured. Despite similar affinity for Dectin-1A, the ability of glucans to induce Dectin-1A mediated calcium influx

and Syk phosphorylation positively correlates with their degree of higher order structure. Chemical denaturation and renaturation of MMW glucan showed that glucan structure determines agonistic potential, but not binding affinity, for Dectin-1A. We explored the role of glucan structure on Dectin-1A oligomerization, which is thought to be required for Dectin-1 signaling. Glucan signaling decreased Dectin-1A diffusion coefficient in inverse proportion to glucan structural content, which was consistent with Dectin-1A aggregation. Förster Resonance Energy Transfer (FRET) measurements revealed that molecular aggregation of Dectin-1 occurs in a manner dependent upon glucan higher order structure. Number and Brightness analysis specifically confirmed an increase in the Dectin-1A dimer and oligomer populations that is correlated with glucan structure content. Receptor modeling data confirms that in resting cells, Dectin-1A is predominantly in a monomeric state. Super Resolution Microscopy revealed that glucan-stimulated Dectin-1 aggregates are very small (<15 nm) collections of engaged receptors. Finally, FRET measurements confirmed increased molecular aggregation of Dectin-1A at fungal particle contact sites in a manner that positively correlated with the degree of exposed glucan on the particle surface. These results indicate that Dectin-1A senses the solution conformation of β-glucans through their varying ability to drive receptor dimer/oligomer formation and activation of membrane proximal signaling events.

Introduction

Overall, *Candida* infections have increased over the past 20 years in the United States [1–5]. It is estimated that 46,000 cases of healthcare-associated invasive candidiasis

occur in the United States annually [6]. The fungal cell wall is composed of an inner layer of chitin, a middle layer of β(1,3:1,6)-D-glucan and an outer layer of N- and O-linked mannans [7]. During infection, the cell wall of *Candida* is an important and relevant virulence factor, playing roles in adhesion, colonization and immune recognition [8,9]. Due to the abundant amount of mannan on the cell wall, β-glucan exhibits a very limited, punctate pattern of nanoscale surface exposure. The extent of this glucan masking is influenced by environmental conditions such as intestinal pH or lactate levels [10,11]. In addition, interactions with neutrophils have been shown to “unmask” the mannose layer through a neutrophil extracellular trap-mediated mechanism [12]. Furthermore, our lab and others have determined that anti-fungal drugs “unmask” the fungal cell wall, which leads to increases in nanoscale regions of glucan exposure and correlates with enhanced host defense [13–15]. Therefore, fungal species use masking as a way to evade recognition of β-glucan by the host’s immune system [16].

β-glucans consist of a β-1,3-linked backbone with side chains of β-1,6-linked units that vary in length and degree of branching [17]. β-glucan forms triple-helical structures through intermolecular hydrogen bonds with two other strands [17–21]. This triple helix conformation has been shown to form with just the β-1,3-linked backbone, however β-1,6-linked side chains play an important role in determination of the triple helix cavity formation through side chain/side chain interactions [21].

β-glucans are known for their biological activities such as enhancing anti-tumor, anti-bacterial, and anti-viral immunity as well as in wound healing [22–25]. The biological activity of glucan is affected by its structure, size, chemical modification, conformation and solubility [26]. Research has found that branching is not required to observe

biological activity, but branching has been shown to enhance binding to the Dectin-1 receptor [27]. In contrast, β-glucan size is thought to play a major role in biological activity with glucans that are shorter than 10,000 Da often being biologically inactive [28,29]. However, despite having similar sizes, glucans can display differences in their biological activities [30–32]. For example, studies have demonstrated that the immunoregulatory activity of laminarin varies between agonistic and antagonistic depending on its physicochemical properties, purity and structure [33]. Furthermore, β-glucans that have a triple helical conformation are more potent agonists of host immune response than single helical glucan [34–37]. We propose that the β-glucan triple-helix conformation plays an important role in determining the biological activity of the β-glucan through modulating the degree of receptor oligomerization upon ligation.

During innate immune recognition of *Candida*, the organization of cell wall ligands and pattern recognition receptors is an important determinant of successful immune activation [8]. The C-type lectin (CTL) anti-fungal immunoreceptors play a central role in the detection of *Candida* during bloodstream infection [38]. Dectin-1A is the main CTL that recognizes the soluble and particulate β-glucan found in the fungal cell wall [39–41]. Dectin-1A is found in myeloid lineage cells, and once activated, it stimulates phagocytic activity, the production of reactive oxygen intermediates and inflammatory mediators. Dectin-1A contains a CTL-like domain, separated from the cell membrane by a glycosylated stalk region, a transmembrane domain and an intracellular cytosolic domain. The cytosolic tail contains half an Immunoreceptor Tyrosine-based Activation Motif (a YXXL sequence with an upstream stretch of acidic amino acids) in its cytoplasmic tail and so is termed a (hem)ITAM receptor [42,43]. Monophosphorylated

ITAM domains poorly recruit and activate Syk for downstream signaling [44], suggesting that hemITAM domains with their single phosphotyrosine site would be poorly activating in a monomeric configuration. Consistent with this hypothesis, another (hem)ITAM bearing receptor, CLEC-2, is reported to require dimerization for its signaling [45]. By analogy to this and other (hem)ITAM receptors, it is hypothesized that Dectin-1A must oligomerize to recapitulate a multivalent binding site for Syk and to facilitate signal transduction [8,45,46]. However, this prediction has not been directly explored for Dectin-1A in live cells at the molecular level with relation to structural determinants of receptor-ligand complex organization and signaling outcomes.

In this study, we propose that factors that induce an aggregated membrane organization of Dectin-1A during activation are very important for determining signaling outcomes of Dectin-1A engagement by β-glucan [45,46]. We hypothesize that ligand structure impacts signaling by determining the membrane organization and spatiotemporal clustering dynamics of Dectin-1A. To test this hypothesis, we stimulated HEK-293 cells transfected with Dectin-1A with a variety of soluble β-glucans that have different structures and sizes. We chose to work in this model system because it provides a simplified platform necessary to investigate the physical biology of Dectin-1A activation by isolating Dectin-1A signaling from the complex milieu of other receptors and other Dectin-1 isoforms expressed in innate immunocytes. Also, this model facilitates the expression of multiple fluorescent protein-tagged Dectin-1A constructs necessary to the work. Using calcium imaging and western blotting assays, our results revealed that Dectin-1A activation is influenced by the β-glucan triple helical structure. Furthermore, our subcellular FRET measurements by Fluorescence Lifetime Imaging Microscopy

(FLIM-FRET), as well as application of fluorescence correlation spectroscopy approaches, revealed dimerization and oligomerization of Dectin-1A when stimulated with highly structured β-glucans. In addition, these dimerization events occurred in fungal contact sites of fungal cells with high glucan exposure. Together, our findings indicate β-glucan structure is required for Dectin-1A to form signaling-competent dimeric and oligomeric membrane aggregates.

Results:

Dectin-1A activation is dependent on the molecular weight of the soluble β-glucan.

β-glucans, existing as insoluble fibers in the cell wall, are likely to have a high degree of tertiary and quaternary structure. So, an encounter with highly structured glucan might be indicative of a pathogen cell wall structure. Furthermore, less structured glucans are encountered by Dectin-1A physiologically [42]. Small soluble circulating glucan can derive from sloughed cell wall material or from dietary absorption [47–50]. However, there is not much known about Dectin-1A's ability to distinguish between highly structured β-glucan found on cell walls of fungal pathogens and less structured glucans found in circulation. Therefore, we examined how Dectin-1A activation is affected by glucans with different quaternary and tertiary structures. To accomplish this, we used high molecular weight (HMW 450 kDa), medium molecular weight (MMW 145 kDa), and low molecular weight (LMW 11 kDa) soluble glucans, in decreasing order of tertiary and quaternary structures, derived from *S. cerevisiae* cell walls. These *S. cerevisiae* glucans

in soluble form or as particulate “zymosan” are common models for stimulation of innate immunocytes by fungal pathogen cell wall glucan. The above glucans have overall very similar composition and structures to *C. albicans* yeast glucan, though relatively minor differences in β-(1,6)-glucan side chain length and branching frequency have been reported between these species [51,52].

Using these glucans, we performed intracellular calcium ($[Ca^{2+}]_i$) measurement experiments using HEK-293 cells transfected with Dectin-1A. We stimulated the cells using either LMW, MMW, or HMW (Fig.1A). We found that large, highly ordered glucans (HMW and MMW) induced more than a two-fold increase in peak amplitude of $[Ca^{2+}]_i$. In contrast, the glucans with a random coil structure (LMW) showed little induction of calcium signaling compared to unstimulated cells. These results indicate that Dectin-1A drives differential Ca^{2+} flux to glucan ligands that vary in size and structure.

To determine how these differently structured soluble glucans impacted cellular patterns of Syk phosphorylation, we stimulated HEK-293 cells expressing Dectin1A-mEmerald with H_2O (vehicle), LMW, MMW, or HMW. Whole cell lysate was collected and Syk phosphorylation was determined by western blot analysis. Likewise, our results show an increase in Syk phosphorylation in the larger, highly structured glucan MMW and HMW compared to unstimulated and LMW stimulated cells (Fig. 1B). Additionally, Syk inhibitors abrogated calcium signaling of Dectin-1A when stimulated with MMW glucan (Fig. 1C). These results indicate that glucans with higher order structure are better able to activate Dectin-1A-mediated Ca^{2+} signaling and that this is a Syk dependent process.

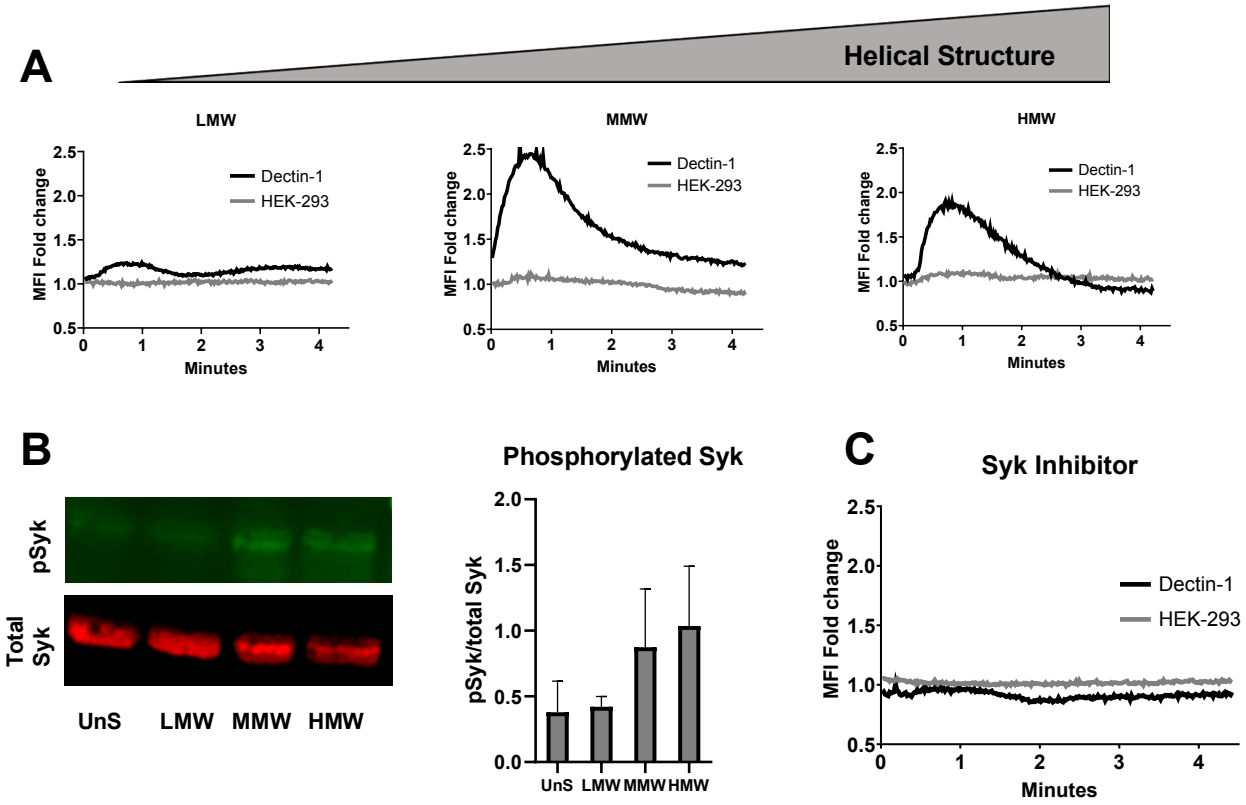

Figure 1. Differential signaling response to soluble β-glucan for Dectin-1A.

(A) HEK-293 cells stably transfected with Dectin-1A were loaded with Fluo-4 and Cell Tracker Deep Red at equimolar concentrations. Cell Tracker Deep Red was simultaneously loaded in order to normalize for changes in cytosolic volume caused from cell movement during observation. Mean fluorescence intensity was observed for Dectin-1A transfected (black) or untransfected (grey) HEK-293 cells stimulated with LMW, MMW, or HMW at 1 ug/ml. (n = 30 per glucan from 3 independent experiments per glucan). Data shown as mean fold change in volume-normalized $[Ca^{2+}]_{intracelullar}$. (B) Cell lysates were collected at 5 min after stimulation and analyzed by Western blotting using antibodies against p-Syk and Syk. The intensity of p-Syk was normalized against total Syk. Representative western blot on the left. Quantification of the western blot data (right) shown as mean ± SD are relative intensity of p-Syk (n = 3). (C) Untransfected (grey) and stably transfected Dectin-1A (black) HEK-293 cells were loaded with Fluo-4 and Cell Tracker Deep Red at equimolar concentrations and treated with Syk Inhibitor at 250 nM and stimulated with

MMW. Mean fluorescence intensity was observed for cells stimulated with MMW at 1 ug/ml. (n = 30 from 3 independent experiments).

β-glucan denaturation does not induce Dectin-1A activation

To specifically determine if the glucan structure affects signaling outcomes, we denatured MMW (highly stimulatory glucan) using DMSO, which inhibits the formation of tertiary structures, thus converting MMW's triple helix structure to a single helical structure [17]. The results showed that when we denatured these glucans, we did not observe calcium signaling in cells expressing Dectin-1A (Fig. 2A). However, when we renatured the glucans by removing DMSO via dialysis we observe partial recovery of calcium signaling. In addition, we confirmed the loss of helical structure via a Congo Red assay. Congo Red specifically binds to β-1,3-D-glucans with a triple helix conformation as their tertiary structure. This binding is detected by bathochromic shift in absorbance maximum from 488 to 516 nm [53]. Our results indicated a loss in glucan structure after denaturation in a DMSO solution that was regained upon renaturation (Fig. 2B). Moreover, we repeated these experiments by stimulating cells with glucan denatured with NaOH or neutralized renatured glucan [17]. Similarly, our results show that denatured MMW does not stimulate Dectin-1A signaling, but agonistic potential of this glucan is partially regained when the glucan is renatured (Fig. 2C). In addition, we confirmed that glucan structure was lost when NaOH was added and regained when neutralized with HCl (Fig. 2D). These results suggest that glucan structure is an important factor in activating a Dectin-1A response.

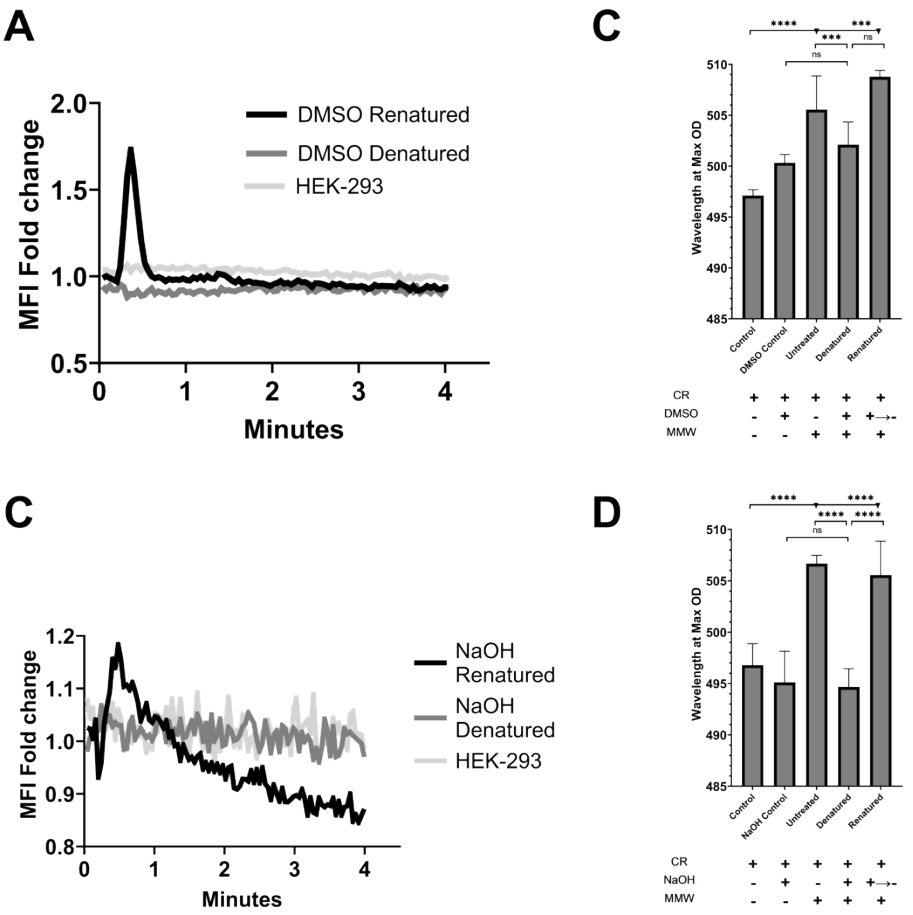

214

215 **Figure 2: Denaturation of highly structured glucan causes it to lose its**

216 **stimulatory potential.**

217 (A) HEK-293 cells stably expressing Dectin-1A or untransfected were loaded with Fluo-4 and Cell Tracker

218 Deep Red at equimolar concentrations. Mean fluorescence intensity was observed for cells stimulated

219 with DMSO denatured/renatured MMW. (n = 30 from 3 independent experiments). (B) 1 mg/ml of MMW

220 glucan was denatured using DMSO and incubated with 8μM Congo Red. Control samples contained

221 Congo Red with and without DMSO to illustrate the extent of red shift attributable to solvent effects alone.

222 Renaturation was accomplished by dialyzing out DMSO 24 hrs prior to the experiment. Data shown as

223 mean ± SD (n = 9 from 3 independent experiments). (C) HEK-293 cells stably expressing Dectin-1A or

224 untransfected were loaded with Fluo-4 and Cell Tracker Deep Red at equimolar concentrations. Mean

225 fluorescence intensity was observed for cells stimulated with NaOH denatured/renatured MMW at 1

ug/ml. (n = 30 from 3 independent experiments). Data shown as mean. (D) 1 mg/ml of MMW glucan was denatured using NaOH and incubated with 8 μM Congo Red. Control samples contained Congo Red with and without Congo Red to assess denaturant effect on the optical properties of the dye, but the presence of denaturant had no significant effect on Congo Red in this case. Renaturation was accomplished by neutralizing NaOH 24 hrs prior to the experiment. Data shown as mean ± SD (n = 9 from 3 independent experiments). Welch's t-test, ** $p<0.001$, *** $p<0.0001$, **** $p<0.000001$.

β-glucan structure and affinity

We considered the possibility that these soluble glucans might have different affinities for Dectin-1A, resulting in differential receptor activation. Thus, we conducted Biolayer Interferometry experiments to determine the binding affinity of these glucans to the carbohydrate recognition domain of Dectin-1A. This was accomplished using a chimeric fusion protein of the carbohydrate recognition domain of Dectin-1A and the human IgG Fc region. An anti-human IgG Fc Capture biosensor tip was used to load this fusion protein. Association and dissociation curves of the soluble glucan were then collected. The results shown in Fig. 3A indicate that all the glucans have approximately nanomolar dissociation constants for Dectin-1A carbohydrate recognition domain despite the previously described differences in signaling [27]. Weight average molecular weights of purified *Saccharomyces cerevisiae* β -(1,3)-glucan fractions vary over an approximate 40-fold range, but there is relatively little difference between these glucans' apparent affinity for the Dectin-1A carbohydrate recognition domain.

Furthermore, to quantify differences in the helical structure possessed by LMW, MMW and HMW glucans, we analyzed the conformational transition of triple helix to random coil of β-1,3-D-glucans through denaturation experiments. Experiments were conducted by denaturing glucans with NaOH at various concentrations in the presence of Congo

Red. Our results show that the amount of glucan tertiary structure scales with molecular weight as measured by the concentration of NaOH required to reduce Congo Red binding to glucan to half-maximal values (Fig. 3B), suggesting that the size of the glucans is correlated with their structure. This result was expected because larger glucans are able to engage in more extensively in interstrand hydrogen bonding interactions that maintain triple helical structures. Together, these results indicate that downstream signaling of the receptor is determined by the structure of the glucan rather than affinity alone.

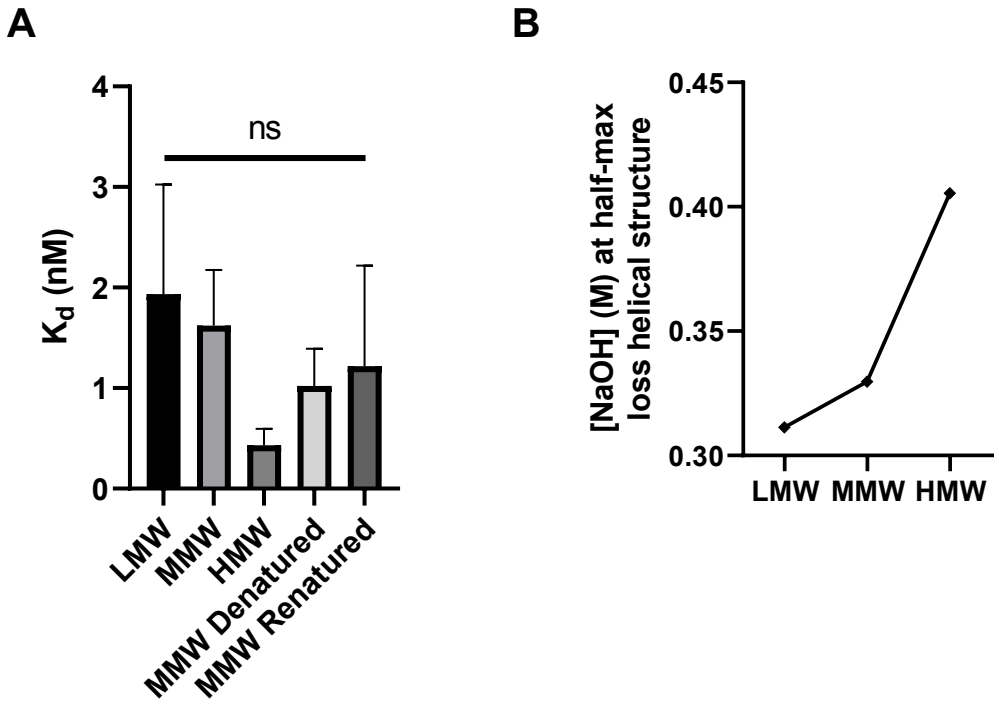

Figure 3: Characterization of fungal cell wall glucans used in this study. Characterization of untreated, denatured and renatured β-glucans.

(A) Biolayer Interferometry experiments were conducted on LMW, MMW, HMW, MMW denatured, and MMW renatured glucans using an anti-human IgG Fc Capture biosensors tip and a Dectin-1A-Fc fusion protein. Data shown as mean ± SD (n = 3 from 3 independent experiments). (B) LMW, MMW, and HMW

β-glucans were denatured using 0M-1M of NaOH in the presence of 8.8 μM Congo Red. Concentration of NaOH at which absorbance decreased to the half-maximal value were plotted. Data shown as mean ± SD (n = 9 from 3 independent experiments); One-way ANOVA test was conducted.

Dectin-1A decreases in diffusion and receptor density when stimulated with highly structured β-glucans

The Stokes-Einstein equation predicts that if a diffusing object increases in hydrodynamic radius, it will slow down proportionally to that change. We measured the diffusion coefficient of Dectin-1A pre/post glucan stimulation to determine whether receptor diffusion coefficient decreased, potentially due to increasing hydrodynamic radius as an initially monomeric receptor formed larger clusters/oligomers. We obtained average diffusion coefficients and spatial number density of our receptor using Raster Image Correlation Spectroscopy (RICS). Previous research has described RICS in more detail [54,55]. Briefly, we generated a volume of excitation using a confocal laser and calibrated this volume using standard fluorophores of known diffusion coefficient. We then observed fluorescent molecules (i.e., Dectin-1A-mEmerald) diffusing in and out of this excitation volume through fluctuation in the number of photons obtained. Experimentally observed florescence correlations at various spatiotemporal lags were then fit to a 2D autocorrelation function to obtain receptor diffusion coefficient and spatial density in the observed membrane.

Using HEK-293 cells expressing Dectin-1A-mEmerald, we conducted RICS measurements before and after stimulation with soluble β-glucans. We determined that cells stimulated with MMW or HMW exhibited a significant decrease in mobility

compared to LMW and unstimulated cells (Fig. 4A). This finding is consistent with an increase in receptor aggregation upon stimulation, which we examine in greater detail below. Moreover, we observed a significant decrease in receptor density after treatment with MMW or HMW, compared to non-simulated or LMW cells (Fig. 4B). This finding might be explained by receptor internalization after stimulation by MMW or HMW. While RICS analysis does use detrending to remove immobile and very low mobility receptor from analysis, we do note that progressive confinement of activated receptors in nascent endocytic structures could also potentially contribute to the decreased apparent diffusion coefficient we observed post-stimulation. So, we proceeded to conduct more detailed membrane biophysical studies to specifically assess the molecular aggregation state of Dectin-1 during stimulation with glucan.

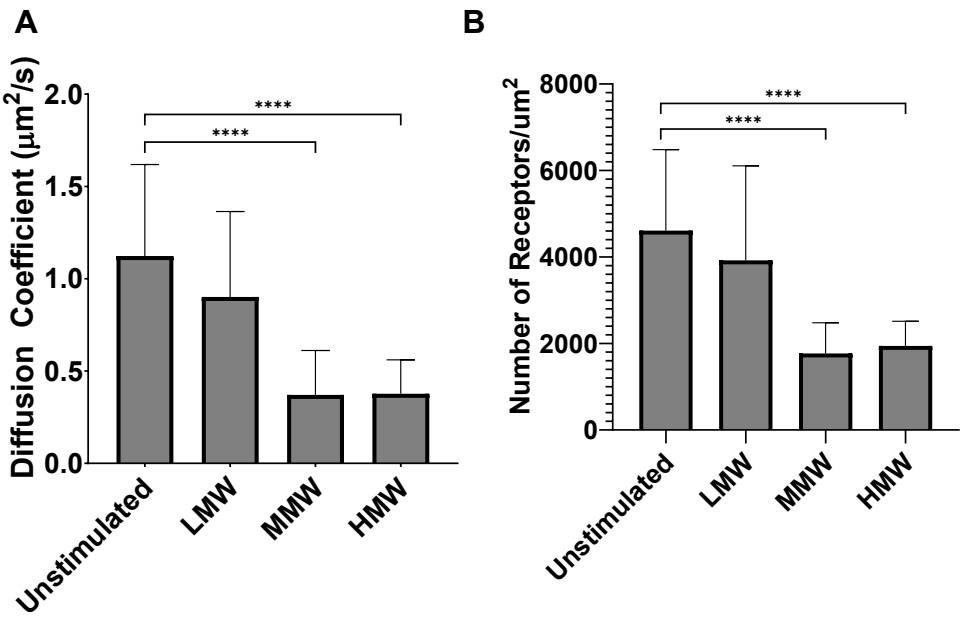

Figure 4: Dectin-1A surface diffusion and receptor numbers decrease when stimulated with highly structured β-glucans.

(A). Raster Image Correlation Spectroscopy (RICS) analysis of fluorescently tagged Dectin-1A expressed in HEK-293 provided average diffusion coefficient and (B) average receptor number for cells that were unstimulated or stimulated with LMW, MMW, or HMW. Data shown as mean ± SD (n = 30); One-Way ANOVA multiple comparison test, **** $p<0.00001$.

Dectin-1A forms dimers/oligomers when stimulated with highly structured β-glucans

The results shown above indicate that the β-glucan structure is an important factor in signaling outcomes. Previous research has shown that other transmembrane CTLs that also contain a (hem)ITAM domain can form homodimers before or upon ligand recognition [56,57]. Furthermore, crystallography studies of the carbohydrate recognition domain (CRD) have shown that Dectin-1A head groups form dimers when laminarin is present [58]. Additionally, size exclusion chromatography with multi-angled light scattering analysis has described Dectin-1 ligand-induced tetramer formation in solution [59]. In line with these ideas, we sought to examine how ligand structure impacts signaling by determining the dimerization/oligomerization of full length Dectin-1A in living cell membranes.

To accomplish this, we first employed Fluorescence-Lifetime Imaging Microscopy for Forster Resonance Energy Transfer (FLIM-FRET). FRET based imaging capitalizes on close proximity of two proteins to visualize protein-protein interactions, including receptor dimerization and receptor-ligand complex formation [60]. FLIM characterizes the duration of a fluorophore's excited state before returning to the ground state. The occurrence of FRET causes rapid quenching of donor fluorescence, so FRET can be

determined by measuring the shortening of donor fluorescence lifetime when in proximity to acceptor. FLIM-FRET offers the opportunity of studying *in vivo* receptor interactions in a direct, spatially resolved manner. We examined Dectin-1A engagement using FLIM-FRET on HEK-293 cells co-expressing fluorescent proteins Dectin-1A-mEmerald (donor) and -mCherry (acceptor). The proteins used for experimental determination of ligation-dependent Dectin-1A aggregation possessed fluorescent proteins on the protein N-terminus (cytoplasmic tail), while a negative control for FRET utilized donor and acceptor-tagged proteins on opposite sides of the membrane. Analysis was conducted on the plasma membrane itself by masking out internal cellular compartments (Fig. 5A). In the experiments, FRET efficiency is a parameter that exhibits an inverse 6th power dependence upon donor-acceptor distance. Donor-acceptor percentage is simply the percentage of all donors that are involved in FRET interactions at a given time. These parameters are determined experimentally by performing bi-exponential curve fits to the observed frequency distribution of donor fluorophore lifetimes, wherein one exponential component represents the population of non-FRET monomeric donors and the other exponential component represents the performance of the donors that are involved in FRET interactions.

First, we characterized the average lifetimes of unstimulated cells expressing several configurations of fluorescent protein tagged Dectin-1A: 1) receptor with donor tag only, 2) co-expression of separate donor and -acceptor tagged receptors with tags placed on opposite sides of the plasma membrane (a negative control containing both fluorescent proteins but in a configuration that does not permit FRET), and 3) co-expression of separate donor and acceptor-tagged receptors with both tags in the cytoplasmic tail of

the receptors (configuration to be used for experimental determination of receptor aggregation by FRET). The observed decay curves were analyzed by performing a bi-exponential fit. For donor only (1) and our negative control (2), we observed a negative amplitude for one of the bi-exponential lifetime fit components, indicating that a mono-exponential fit was a more appropriate method of analysis. Our results showed that when acceptor was not present, we see an average of 2.4 ns lifetime (Fig. 5B). Negative controls with donor and acceptor on opposite sides of the membrane yielded similar lifetime values. FLIM data from cells with co-expression of donor or acceptor-tagged (cytoplasmic tail) Dectin-1A was fit bi-exponentially with the first component fixed to the donor only lifetime (2.4 ns) and the lifetime of the second component was reported. In this case, resting cells exhibited a decrease in the lifetime of the donor to 0.41 ns indicating that some basal level of intermolecular Dectin-1 close proximity interactions were being observed in unstimulated cells. The existence of this basal FRET signal is interesting, and the potential sources and interpretation of this observation are considered in a section below. However, we first focused on assessing ligation-dependent changes in Dectin-1A's molecular aggregation state as influenced by various glucans and measured by FRET.

When we stimulated cells expressing Dectin-1A with donor and acceptor on the cytoplasmic face of the membrane using MMW (Fig. 5D) or HMW (Fig. 5E), we saw a significant increase in the number of receptors undergoing FRET (Donor-Acceptor population) from 15% before stimulation to a maximum of 30% after 5 minutes of stimulation, with observations starting at one minute post-stimulation. However, there was not a significant change in FRET efficiency before and after stimulation. On the

other hand, when we stimulate with LMW (Fig. 5C) or denatured MMW (Fig. 5F), we see no significant change in FRET efficiency or donor-acceptor population. We interpret the high and constant FRET efficiency for the population of receptors engaged in FRET interactions to mean that Dectin-1A in its aggregated state is in a close, well-defined configuration that does not permit a wide range of separations between donor and acceptor tags, leading to a constant FRET efficiency for the donor population that does attain this FRET-capable configuration. However, the size of the population of receptors engaged in these close molecular aggregates does change as a result of stimulation with glucan. These results suggest that the highly structured soluble glucans allow for an increase in Dectin-1A dimerization or oligomerization to occur, which directly correlates with the amount of receptor activation and signaling observed.

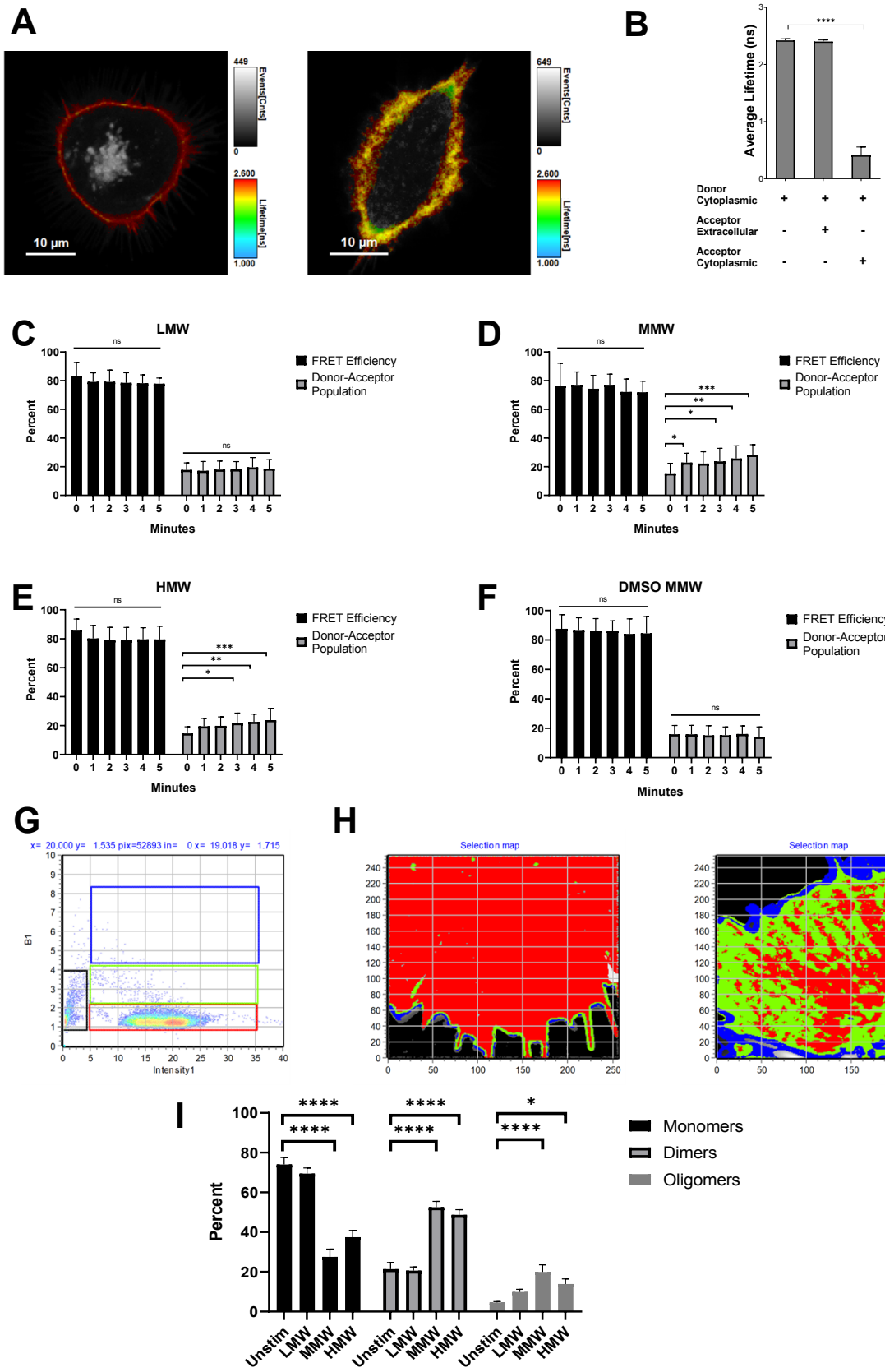

Figure 5: Highly structured β-glucans induce dimerization of Dectin-1A.

(A) Representative lifetime image of HEK-293 cell transfected with Dectin-1A-mEmerald (left panel) or cotransfected with Dectin-1A-mEmerald and Dectin-1A-mCherry (right panel). (B) Average lifetime of HEK-293 cells expressing donor only on the cytoplasmic face, donor expressed on the cytoplasmic side and acceptor on the extracellular side or donor-acceptor placed on the cytoplasmic side of the membrane. Decay curves for donor only and the negative control were mono-exponentially fit while cytosolic donor and acceptor decay curves were bi-exponentially fit with the first component fixed to 2.4 and the second component shown. Data shown as mean ± SD (n = 15 cells); Welch's t-test, **** p<0.00001. (C) FRET efficiency and donor-acceptor population of cells stimulated with LMW, (D) MMW, (E) HMW, or (F) DMSO denatured MMW. Data shown as mean ± SD (n = 15); One-way ANOVA multiple comparisons Dunnett test, * p<0.05, **p<0.01, ***p<0.001. (G) Brightness vs intensity 2D histogram with the selected pixels that contribute to the background (black), monomers (red), dimers (green), and tetramers (blue) in the image. (H) Representative selection map of HEK-293 cells expressing Dectin-1A-mEmerald unstimulated (left) or stimulated with MMW β-glucan (right) in which Dectin-1 aggregation states are defined by colored boxes selected in the Brightness vs intensity histogram. (I) Percentage of aggregates in Dectin-1A-mEmerald receptors and receptor ligand complexes obtained from N&B analysis before or after stimulation. Data shown as mean ± SD (n = 30); One-way ANOVA multiple comparisons Dunnett test, * p<0.05, **** p<0.00001.

To better characterize the aggregation states accessible to Dectin-1A, we conducted a Number and Brightness analysis (N&B) on HEK-293 cells expressing Dectin-1A-mEmerald. Previous research has described N&B more in depth [61–63]. Briefly, N&B analysis focuses on fluctuation of detected emission photons originating from fluorescent molecules that pass through a known observation volume. Statistics of fast fluctuations of the intensity at each pixel can be used to determine the number and intensity of the particles diffusing through the observation volume. For example, if the fluorescent proteins diffuse as a tetrameric protein, we expect to observe emission

intensity fluctuation with four times more photons relative to a monomeric fluorescent protein diffusing through the excitation volume. Receptor aggregation was observed by stimulating these cells with soluble glucans. A brightness vs intensity 2D histogram of each pixel in a time series was developed, and selection boxes were drawn to represent monomers (red box), dimers (green box) and oligomers (blue box) (Fig. 5G). Dectin-1 aggregation state maps of representative untreated (Fig. 5H left panel) and MMW-stimulated cells (Fig. 5H right panel) were generated using this color scheme. We observed a significant increase in pixels with a dimer and oligomer brightness in cells stimulated with MMW and HMW compared to cells that were unstimulated or LMW stimulated (Fig. 5I). N&B analysis revealed that dimers of Dectin-1A account for the majority of aggregated state Dectin-1.

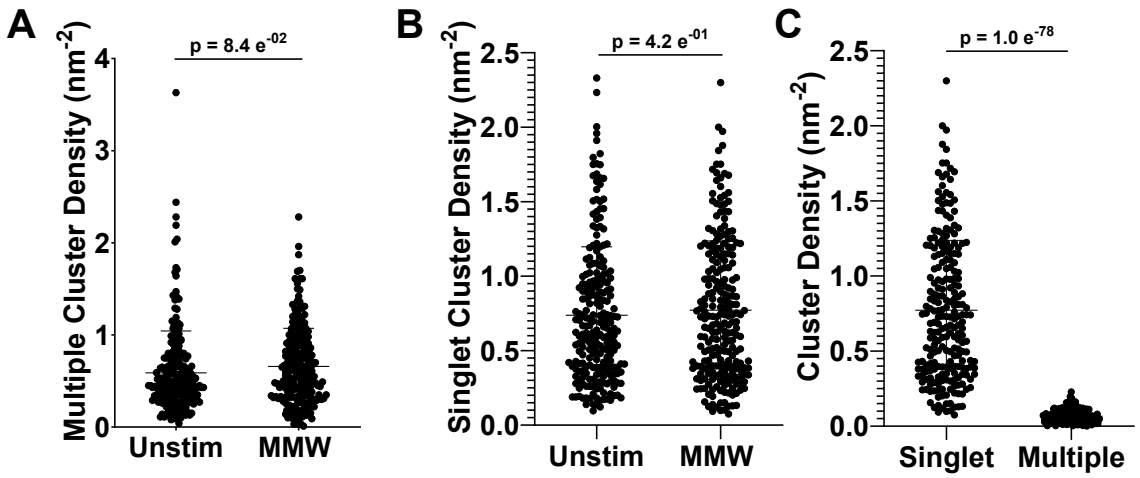

Figure 6: Dectin-1A does not form large scale aggregation when stimulated with highly structured β-glucan.

(A) Multiple cluster density of dSTORM analysis of HEK-293 cells expressing Dectin-1A unstimulated or stimulated with MMW. A singlet cluster is a cluster of localizations determined to arise from 3 or more

individual Dectin-1 proteins. (B) Singlet cluster density of DSTORM analysis of HEK-293 cells expressing Dectin-1A unstimulated or stimulated with MMW. A singlet cluster is a cluster of localizations determined to arise from a single Dectin-1 protein, or potentially >1 Dectin-1 protein within sub-resolution displacements from one another. (C) Density of singlet and multiple cluster of Dectin-1A expressing HEK-293 cells treated with MMW. Data shown as mean ± SD (n = 34) with significance assessed by Student's t Test.

β-glucan induced Dectin-1A aggregates are below 15 nm in size

While FRET-based observations and N&B analysis clearly show the presence of ligand-induced, molecular-scale aggregation (e.g., dimerization) of Dectin-1A, these methods are not as well suited to discern the existence of larger scale aggregation of the receptor (e.g., clusters of tens to hundreds of receptors). We used direct Stochastic Optical Reconstruction Microscopy (dSTORM) coupled with Hierarchical Single-Emitter hypothesis Test (H-SET) analysis [13] to resolve aggregation of Dectin-1A before and after stimulation with MMW glucan. This localization super resolution microscopy technique accurately resolves objects from the diffraction limit (~300 nm, the resolution limit of conventional fluorescence microscopy methods) or above, down to ~15 nm (a typical resolution limit of dSTORM using our configuration). H-SET analysis detected sites of Dectin-1 labeling as "singlet" objects or "multiple" clustered objects. Multiple clustered objects are those with three or more resolvable individual Dectin-1 molecules. Singlet objects are those that appear to contain only a single, resolvable Dectin-1 labeling event, though it is possible that multiple Dectin-1 molecules in very close proximity (<15 nm separation) would be unresolvable and appear as a singlet object. We detected no significant change in the density of singlet objects or multiple object

clusters before vs after MMW glucan stimulation (Fig. 6A,B; Supplemental Fig. 1). Consistent with our previous findings, singlet exposures greatly outnumber multiple exposures on the cell wall surface (Fig. 6C). Localization number per multiple cluster object did not change with stimulation (Supplemental Fig. 1), suggesting no change in the number of receptors in such objects. Ripley's K analysis suggests clustering up to the ~50 nm length scale but not at longer length scales (Supplemental Fig. 1). In the context of the previous findings showing molecular aggregation at very small scales, potentially below the resolution limit of dSTORM, we concluded that dSTORM results indicated that the Dectin-1A aggregates formed upon glucan stimulation are quite small and below the resolution limit of dSTORM (<15 nm length scale). Because this places an upper bound on the size of ligand-induced Dectin-1 clusters and we can estimate that the CRD of Dectin-1 occupies an area approximately 25 nm^2 (PDB: 2BPD; [58,64]), we conclude that Dectin-1 aggregation after MMW glucan stimulation most likely involves collections of not more than ~7 receptors.

Dectin-1A is predominantly monomeric in resting cell membranes

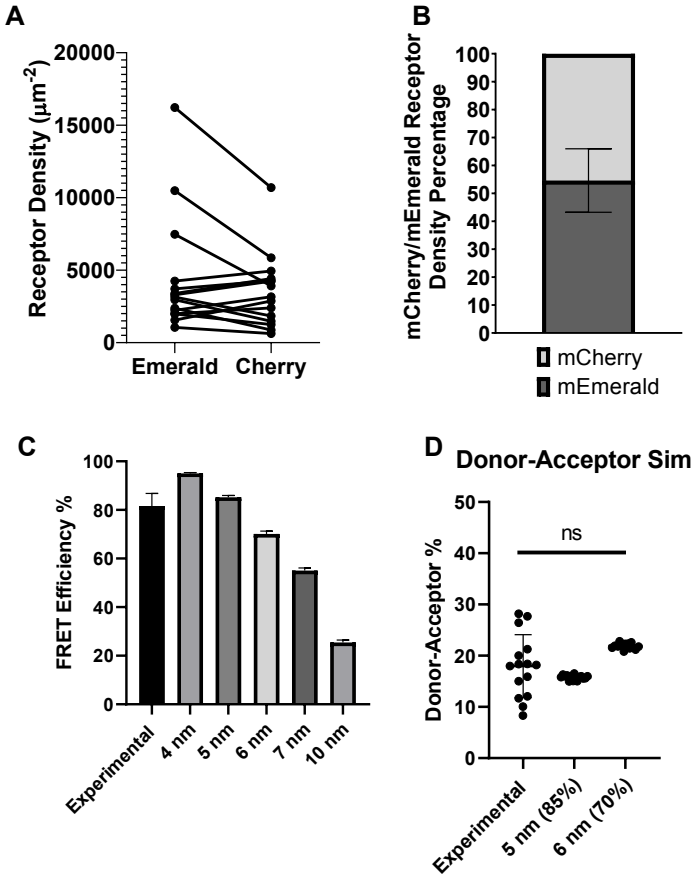

463

464 **Figure 7 Dectin-1A collisional diffusion FLIM-FRET model:**

465 (A) Receptor density of HEK-293 cells co-expressing Dectin-1A-mEmerald and -mCherry. (B) Ratio of
466 mEmerald/mCherry expression in unstimulated HEK-293 cells. (C) FRET Efficiency (FE) of Dectin-1A
467 donor/acceptor simulated at different maximum intermolecular radial distances and experimental
468 observations of FRET in resting cells. (D) Percentage of donors undergoing FRET (Donor-Acceptor
469 Population) for experimental results from resting cells and FLIM FRET simulations at 5 and 6 nm
470 maximum radii. Data shown as mean ± SD (n = 15 independent simulations or experimental observations
471 on cells, respectively); One-way ANOVA multiple comparisons Dunnett test.

472

FRET-based measurements and N&B analysis reported that the large majority of Dectin-1 is distributed as monomers in unstimulated cells. However, a minority population of receptors in states indicative of some close intermolecular interaction was observed in these cells by both techniques. This may represent random collisional interactions between Dectin-1 molecules, with no stable receptor oligomer formation. For instance, FRET may be observed from random collisional interactions without requiring stable receptor aggregation. Alternatively, it is possible that a small fraction of Dectin-1 does form dimers or oligomers, even in the absence of glucan. It is difficult to conclusively distinguish between these alternative hypotheses using only the experimental results shown above. Therefore, we created a computational model of fully monomeric Dectin-1 undergoing Brownian 2D diffusion to predict FLIM-FRET results anticipated from a purely monomeric receptor system. We determined the receptor density of both donor and acceptor for HEK-293 cells coexpressing Dectin-1A mEmerald/mCherry by RICS analysis (Fig. 7A). Our results indicated on average Dectin-1 co-transfected cells contain 54.6% mEmerald and 45.4% mCherry (Fig. 7B). Therefore, our model was populated by equal proportions of donor and acceptor tagged Dectin-1 molecules. Their diffusion coefficients were parameterized using data from Fig. 4. The model calculated FRET rates for all donor-acceptor pairs within a specified maximum radial distance. The maximum radius for experimental FRET observation is limited by signal-to-noise ratio and other factors. To avoid simulating FRET measurements at experimentally unrealistic radii, we varied the maximum donor-acceptor radial distance in a range of 4-10 nm and constrained the model with an experimentally realistic maximum radius for calculation of FRET. We compared

simulated and experimental FRET efficiencies and used maximum radii for simulation that yielded FRET efficiency in best agreement with observed FRET efficiency on resting cells. Our results show our experimental FRET efficiency values match model predictions closely at maximum radii between 5 and 6 nm (Fig. 7C). Simulations at these radial parameters were then compared to experimental results with respect to the donor-acceptor population percent that they predicted.

We used the predictions of this computational model to test the hypothesis that random collisional FRET interactions of donors and acceptors is sufficient to explain the basal FLIM-FRET signal observed experimentally in resting cells. If this model, which incorporates only collisional interactions between donors and acceptors, predicts a percent of donors undergoing FRET interactions with acceptors that matches the experimentally observed value, we would consider that collisional interactions alone are sufficient to explain the observed basal FRET signal. However, if the model predicts a value significantly below that experimentally observed, we would propose that a minor fraction of Dectin-1 molecules may participate in aggregates on cell membranes, even in the absence of glucan. Using simulations with radial values of 5 and 6 nm, our results indicate that the experimentally observed amount of Dectin-1 receptors participating in FRET interactions (Donor-Acceptor population) prior to stimulation match closely to our simulated results (Fig. 7D). This indicated that the FRET signal we observe prior to stimulation was attributable to random collisional interactions of monomerically diffusing receptor expected at the Dectin-1A expression level present in our experimental system.

519 **Dectin-1A dimer/oligomer and contact site formation is more efficient with cells**
520 **incubated with *C. albicans* containing high glucan exposure.**

521 Throughout the article, we have focused on experiments using soluble glucans. In order
522 to show Dectin-1 aggregation occurs during fungal cell recognition, we used high
523 (TRL035) and low (SC5314) β-glucan exposing *C. albicans* strains and examined
524 Dectin-1 aggregation occurring at the contact sites with these yeast. TRL035 has been
525 previously shown to have high glucan exposure compared to SC5314 [65]. In addition,
526 our representative images show TRL035 forming a phagocytic cup more efficiently then
527 SC5314 (Fig. 8A). We observed no significant difference in FRET efficiency between
528 any conditions tested (Fig. 8B), similarly to our observations with soluble glucan. This
529 finding is consonant with a larger trend in the data presented in this report where FRET
530 efficiency is relatively constant and differences in glucan recognition seem to be mainly
531 associated with differences in the proportion of Dectin-1A molecules engaged in
532 molecular aggregates. Our results further show that HEK-293 cells co-transfected with
533 Dectin-1A-mEmerald and Dectin-1A-mCherry exhibit an increase in the proportion of
534 aggregated-state receptors from approximately 15% in non-contact site membrane to
535 about 25% in contact sites of high glucan exposing yeast TRL035 and glucan particles
536 (Fig. 8C). Interestingly, we did not measure a significant increase in receptor
537 aggregation between non-contact membranes and contact sites with low glucan
538 exposing SC5314. The significance and interpretation of these findings is further
539 discussed below. These results suggest that larger glucan exposure results in an
540 increase of Dectin-1 in molecular aggregates with associated signaling, resulting in a
541 more efficient recognition of yeast by the Dectin-1A receptor.

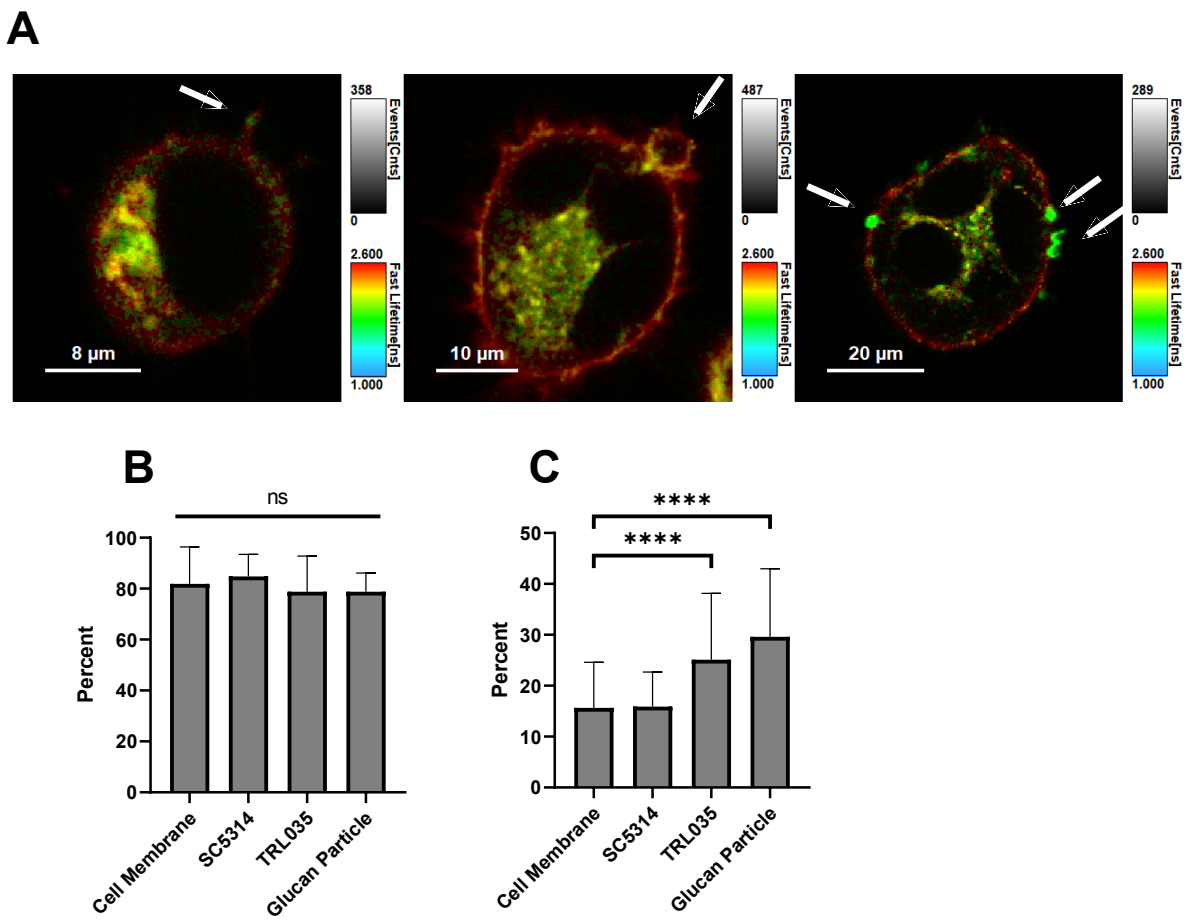

542

543 **Figure 8: Dectin-1A forms more oligomers at fungal contact sites with high β-**

544 **glucan exposure.**

545 (A) Representative lifetime images of HEK-293 cells co-transfected with Dectin-1A-mEmerald and Dectin-

546 1A-mCherry incubated with SC5314 (left panel), TRL35 (middle panel) or particulate glucan (right panel).

547 Transition from redder to greener pixels at contact sites is indicative of increased FRET interactions

548 between Dectin-1 receptors. (B) FRET efficiency and (C) donor-acceptor population of cell membranes

549 with no fungal contact, SC5314 (low glucan exposure), TRL35 (high glucan exposure), or particulate

550 glucan. Data shown as mean ± SD (n = 15); One-way ANOVA multiple comparisons Dunnett test, ****

551 $p<0.00001$.

552

Discussion

Our results demonstrate that the structure of β-glucan impacts receptor signaling by determining the membrane organization and molecular aggregation state of Dectin-1A. We showed that glucans with higher order structure are better able to activate Dectin-1A signaling. Upon activation by stimulatory soluble glucan, Dectin-1A enters aggregated states that contain dimers and higher order oligomers, but these appear to remain as small nanoscale domains containing relatively small numbers of receptors. Comparison of computational modeling and experimental FLIM-FRET data confirms that Dectin-1A exists in a monomeric state in resting cells. Further, monomeric receptors oligomerize and aggregate in a fashion that is dependent upon glucan higher order structure and correlated with the magnitude of membrane proximal signaling downstream of Dectin-1. Finally, we observed that a similar process of increasing Dectin-1 aggregation is seen at contact sites with yeast and fungal-derived particles, and the amount of aggregated state Dectin-1A correlates with the degree of glucan exposure on the surface of the particle. We have summarized all of our quantitative findings in numerical form in Supplemental Table 3 for convenient reference.

β-glucan is widely distributed on various fungal species as an insoluble component of the cell wall. The soluble form is produced when macrophages recognize fungal surfaces and release enzymes that degrade cell wall glucans [47,48]. These soluble glucans are commonly found in circulation in the serum of patients with fungal infections [49,50]. β-glucans possess three different structures: low molecular weights possess a random coil structure while high molecular weight glucans possess either a single or triple helical structure [66]. Furthermore, studies have shown that the complexity of β-

glucan is associated with stronger immunostimulatory effects [17,27,29,66,67]. However, these ensemble-based studies concern β-glucan stimulation at the population level. Therefore, we took a single cell approach to understand nanoscale glucan signaling dynamics using glucans that vary in size and structure. In line with previous studies, our results revealed that Dectin-1A activation is influenced by the β-glucan triple helical structure. Together, these findings demonstrate that β-glucan impacts receptor signaling due to structure and not merely through its affinity or size.

A previous study indicated that the amount of glucan triple helical structure positively correlates with its binding affinity for receptors on human promonocytic cells, and biochemical evidence suggested that glucans with more triple helical content exhibit greater selectivity in receptor interactions on these cells [27]. This evidence suggests that glucan higher-order structure does impact the character of ligand-receptor interactions in the context of whole cells. We hypothesized that glucan structure impacts signaling by modulating the frequency of Dectin-1A dimer/oligomer formation, thus creating sites where Syk could be better recruited via interactions of its SH2 domains with the phosphorylated YXXL sequence in the Dectin-1A cytosolic tails. Our FLIM-FRET results reveal that Dectin-1A enters a state of greater molecular aggregation when stimulated with β-glucans possessing higher ordered helical structure. These results agree well with a previously described model of (hem)ITAM signaling from another C-type lectin receptor, CLEC-2, in which the minimum signaling unit for CLEC-2 is a phosphorylated dimer, enabling recruitment of a single molecule of Syk [45].

In addition, our FLIM-FRET results suggested possible intermolecular interactions between Dectin-1 proteins even before stimulation with β-glucan. We considered this possibility carefully because receptor oligomeric states exist in the basal state for some other C-type lectin receptors, such as DCSIGN, DNGR-1, and NKp80 [68–71]. However, Dectin-1A does not contain cysteine residues in its stalk region which have been shown to be important in the dimerization of other C-type lectin receptors. Therefore, it is considered that Dectin-1A, like CLEC-2, is more likely to experience ligand-induced aggregation in the form of non-disulfide-linked homodimers instead [70–72]. Our experimental data did show evidence of close molecular interactions between individual Dectin-1A proteins in the membrane, but comparison with modeling results indicates that this signal is attributable to an expected level of very transient collisional interactions between the receptors, given the receptor density and diffusion coefficient present in our experimental system. Therefore, our membrane biophysical investigations are most consistent with a model wherein transient Dectin-1A interaction events may occur in resting cell membranes, but upon ligation by highly structured glucans, dimers and small oligomers are stabilized, which drives increased efficiency of Dectin-1 signaling.

Throughout our experimental FLIM-FRET datasets, we repeatedly observed significant glucan induced shifts in the percentage of donors that were participating in FRET interactions, but little change in FRET efficiency as a function of glucan stimulation. FRET efficiencies measured were relatively constant across experimental conditions and also quantitatively fairly high (typically about 75-85%). This suggests that when FRET was experimentally observed, it was derived from close intermolecular

interactions of neighboring Dectin-1A molecules, such as might be expected in an ordered molecular aggregate, such as a dimer or tetramer. In such an aggregate, donor-acceptor separation distances are not free to vary over a wide range because, while the aggregate state exists, those distances are determined by the ordered structure of the protein-protein complex. Therefore, we think that our data is consistent with a model wherein Dectin-1 transitions between monomeric forms and ordered intermolecular aggregate states. We observe that glucan structure controls Dectin-1 aggregation primarily by changing the fraction of receptors in aggregated states.

Similarly, our N&B results indicate a formation of dimers and oligomers in cells stimulated with glucans possessing significant higher order helical structure. These findings are directly in line with previous crystallographic studies that show monomeric Dectin-1A CRD in the absence of glucan but able to form dimeric complexes in the presence of β-glucan [58]. In addition, other studies have shown a ligand-induced cooperative formation of Dectin-1 CRD tetramers [59]. However, these studies were performed with truncated receptor ectodomain proteins outside the context of living cell membranes, so our findings better establish and define the relevance of such ordered aggregate states to full length Dectin-1 in a more physiologically realistic context.

Our dSTORM super resolution results indicate a lack of large aggregates forming. Because of the resolution limit of 15 nm, it is possible that our dSTORM analysis is limited in its ability to resolve the formation of small aggregates. Furthermore, it is also possible that in the soluble form, receptors are internalized rapidly, not allowing for plasma membrane aggregate formation to be observed. In the case of glucan encountered at the yeast cell wall, Dectin-1 aggregates may form at the host-fungal cell

644 contact site, where engaged receptor is physically prevented from quickly internalizing.
645 A previous work demonstrated the organized recruitment of Dectin-1 to a “phagocytic
646 synapse” with glucan particles, where Dectin-1A interactions were presumed to occur
647 and give rise to signaling [73]. Our study directly demonstrates the aggregation of
648 Dectin-1 at these surface interaction sites in living cells. In the future, these studies may
649 be expanded to better characterize the dynamics of receptor recruitment, aggregation
650 and internalization at phagocytic synapses with fungal pathogens.

651 To determine if this phenomenon occurs at early time points of fungal recognition, we
652 conducted FLIM-FRET experiments of contact sites of *C. albicans* lab strain SC5314
653 and our clinical isolate TRL035. TRL035 has been previously described as having
654 higher glucan exposure compared to SC5314 due to a 3-fold reduction of mannan
655 structure [65]. Our results indicate an increase in Dectin-1A aggregation at the contact
656 sites of yeast that have higher glucan exposure as well as contacts with particulate
657 glucan. We were only able to observe increases in contact site Dectin-1A aggregation
658 state for yeast and fungal particles with unusually high glucan exposure for *C. albicans*
659 yeast. No such increase over non-contact membrane sites was detectable at contact
660 sites with SC5314 *C. albicans* yeast (low glucan exposure due to efficient glucan
661 masking). This observation does not necessarily imply that there is no Dectin-1
662 aggregation in response to glucan exposures on *C. albicans* SC5314. The fraction of
663 Dectin-1 in aggregated states vs the monomeric state may be small enough to be below
664 our limit of detection by FLIM-FRET in this case.

665 Glucan exposure magnitude is thought to be regulated by masking of glucan by outer
666 cell wall mannoproteins, providing a very effective mechanism of fungal immune

667 evasion in *C. albicans*. Our previous optical nanoscopy studies of glucan exposure on
668 *C. albicans* SC5314 and TRL035 have revealed a severely limited cell wall surface area
669 containing exposed glucan that is capable of multivalent interaction with Dectin-1. It is
670 reasonable to presume that these limited sites of multivalent glucan exposure may be
671 the rate limiting factor in determining Dectin-1 aggregation and signaling at phagocytic
672 synapses. Our previous studies allow us to estimate multivalently-engaging glucan
673 exposure site density and area (per exposure site) as follows: SC5314—1 μm^{-2} density,
674 $6.61x10^{-4}$ μm^2 area; TRL035—4 μm^{-2} density, $9.62x10^{-4}$ μm^2 area [65]. We previously
675 measured the total area of contact sites between *C. albicans* and human immature
676 dendritic cells as ~10 μm^2 [74]. Finally, we have estimated (see above) that one Dectin-
677 1 CRD occupies a footprint of ~25 nm^2. From these figures, we can estimate that one
678 typical 10 μm^2 phagocytic synapse would contain a maximum of ~264 multivalently
679 engaged Dectin-1 proteins for *C. albicans* SC5314, and maximum ~385 multivalently
680 engaged Dectin-1 for TRL035. For comparison, at the observed receptor density in our
681 model (Fig. 4), we would expect ~46000 total Dectin-1 proteins to be present in this
682 entire phagocytic contact membrane. However, an important caveat is that, in our model
683 system, we noted that SC5314 phagocytic synapses were much smaller than those for
684 TLR035. A smaller contact site would reduce the number of multivalently engaged
685 receptors in SC5314 synapses considerably relative to the above estimates—perhaps
686 decreasing the number of multivalently engaged Dectin-1s by approximately an order of
687 magnitude. So, these estimates emphasize Dectin-1 system is highly sensitive and able
688 to drive signaling responses when only a few hundred receptors, corresponding to less
689 than 1% of the total contact site resident Dectin-1 proteins, are aggregated in the

690 phagocytic synapse. Moreover, these results and estimates suggest that fungal
691 recognition requires the Dectin-1 system to engage in a search for rare sites of
692 multivalent interaction with glucan. It is very likely that Dectin-1 must cooperate with
693 other anti-fungal receptors for the purposes of building and stabilizing the fungal contact
694 wherein this search process operates. This aspect of receptor cooperativity is an
695 aspect of fungal recognition not present in our simplified experimental model. Future
696 studies may productively address how other CTLs (i.e., DC-SIGN and CD206, which
697 establish firm adhesion to abundant fungal surface mannans) may physically and
698 biochemically assist in Dectin-1's search for rare ligand by building and maintaining a
699 robust phagocytic synapse.

700 Previous research has shown that glucan unmasking can be caused by enzymatic
701 degradation of the mannoproteins by macrophages after initial recognition of the fungal
702 cell [47,48]. Furthermore, anti-fungal drugs have also been shown to unmask fungal cell
703 walls that then allow for clearance by the host's immune system [13,14]. Our previous
704 studies have shown that the vast majority of cell wall glucan exposures are only large
705 enough to engage a single Dectin-1 CRD, suggesting that most glucan exposures may
706 not be able to multivalently engage Dectin-1. The fact that most glucan exposure sites
707 on SC5314 *C. albicans* yeast are of this type may explain why we are not able to see
708 much Dectin-1A aggregation in their contact sites. In contrast, we have reported that
709 TRL035 has an increased density and size of glucan exposures capable of multivalent
710 Dectin-1 interactions, which agrees with our finding of increased molecular aggregation
711 of Dectin-1A at contact sites with TRL035 in the present study. Overall, our findings
712 have been consistent with a model wherein the ability of Dectin-1 to find and aggregate

713 at multivalent exposures of glucan on fungal cell wall surfaces is a critical determinant of
714 Dectin-1 dependent innate immune fungal recognition.

715 Overall, these findings indicate that β-glucan structure is required for Dectin-1A to
716 undergo Syk-dependent signaling. Here we provide evidence in support of a model in
717 which highly structured glucans induce dimerization and/or oligomerization of the
718 receptor. This allows their (hem)ITAM domains to become close enough to allow for the
719 activation of Syk, leading to further signaling cascades. Greater understanding of
720 receptor activation is required to better understand the role of Dectin-1A and its agonists
721 as a potential way forward for adjuvant and immunotherapy development. Furthermore,
722 given the worldwide burden of candidiasis, further experimentation is required to better
723 understand the role of Dectin-1A in recognition of these pathogens.

724

725 **Materials and Methods:**

726 **Cell Culture**

727 The HEK-293 (ATCC, #CRL-1573) cell line was maintained in Dulbecco's minimum
728 essential medium supplemented with 10% Fetal Bovine Serum (FBS), 1%
729 penicillin/strepromycin, 2mM L-glutamine, 11mM Sodium pyruvate, and 1% HEPES.
730 Cells were maintained in an incubator at 37°C at 5% CO_2 levels. Cells were maintained
731 at 37°C, 5% CO_2, and 75% humidity during imaging.

732 **Plasmid**

Emerald-Dectin1A-N-10(Addgene plasmid, #56291), Emerald-Dectin1A-C-10 (Addgene plasmid # 54057), mCherry-Dectin1A-C-10 (Addgene plasmid # 55025), and mCherry-Dectin1A-N-10 (Addgene plasmid # 55026) was a gift from Michael Davidson. Transfection with plasmids was performed using standard protocols of Fugene 6 (Promega, #E2691). pUNO1-hDectin-1A (Invivogen) was stably transfected into HEK-293 cells for use in our calcium studies. HEK-293 cells were selected using Geneticin (G418 Sulfate) (Thermo-Fischer, #10131035) at 400 ug/ml for 2 weeks.

Fungal Growth/Preparation

C. albicans SC5314 (ATCC, MYA-2876) or TRL035 yeast cells were grown from glycerol stock, stored at −80°C. Samples were grown in YPD, for 16 h at 37°C in an orbital shaker at 250 rpm to mid log phase. Following a 3-minute centrifugation at 6000 rpm, the supernatant was removed, and the cells were resuspended in 4% paraformaldehyde and sterile phosphate-buffered saline (PBS) for 15 minutes. The cells were centrifuged and washed with sterile PBS 3 times. The cell concentration was then determined using a disposable hemocytometer (C-Chip; Bulldog Bio catalog no. DHC-N01). 3.5 x10^6 cells were resuspended in 1 ml of PBS. 100 µl of the solution was added to HEK-293 cells in 35 mm dishes 15 minutes prior to imaging.

Soluble Glucans Chromatographic Analysis

Low (LMW, 11 kDa), medium (MMW, 145 kDa), and high (HMW, 450 kDa) molecular weight β-1,3;1-6-glucan extracted from *S. cervisiae* cell wall was generous gift from ImmunoResearch Inc. (Eagan, MN). The molecular weight was assessed by gel permeation chromatography (GPC) and multi angle light scattering (MALS). Samples

(100 µg) were injected and eluted with a mobile phase of 0.15 M sodium chloride containing 0.02% sodium azide at a flow rate of 0.5 mL/min using two Waters Ultrahydrogel 500 columns and one Waters Ultrahydrogel 250 column connected serially. The samples were run with the column temperature at 18°C. The Mw was calculated using Wyatt Astra software using data resulting from measurements of the angular variation of scattered light using the MALS detector coupled with the concentration measured by the DRI signal.

Soluble Glucan Linkage Analysis

Desalted and lyophilized samples of the fractions were dissolved in dimethylsulfoxide (DMSO) and treated with NaOH and methyl iodide to methylate all free hydroxyl groups [75]. The methylated material was purified by extraction with dichloromethane and washing with water. The purified material was then hydrolyzed with trifluoroacetic acid, the reducing ends of the resulting sugars were reduced with $NaBD_4$, and then the resulting free hydroxyl groups were acetylated with acetic anhydride. The mixture of partially methylated alditol acetates was analyzed by gas chromatography. Each derivative corresponding to a particular linkage has been identified by a characteristic retention time and mass spectrum using a mass detector. The relative amount of each derivative was measured by gas chromatography with flame ionization detection. The areas obtained for each observed peak are used to calculate the relative amounts of each type of linkage found in the sample (Table 1). The 3,6-linked residues represent branch points.

Table 1.

	LMW	MMW	HMW
Terminal Glucose	6.4	5.1	5.4
3-Glucose	87.5	87.6	84.6
3,6-Glucose	3.2	3.8	4.0
6-Glucose	1.3	2.2	3.2
4-Glucose	0.1	0.2	0.1
Other	1.5	1.1	2.7

777

778 **Soluble Glucan ^{1}H NMR Spectroscopy**

779 The samples were dissolved in DMSO-d6/D2O (6:1 by volume) at 100°C for 1 h.
780 ^{1}HNMR Spectra were recorded at the University of Minnesota Department of Chemistry
781 NMR lab on a Varian UNITYplus-300 spectrometer at 80°C. The spectra were collected
782 at 300 MHz with 32 scans, a relaxation delay of 1.5 seconds, a pulse of 45°, an
783 acquisition time of 2.0 seconds, and a spectral width of 5999 Hz. Table 2 provides ^{1}H
784 NMR chemical shifts in all three glucans used in this study as well as literature values
785 [76]. These data, taken together with other characterization methods used, do confirm
786 that the structure of the polysaccharides used in this study conforms to expected results
787 from fungal cell wall glucans (Table 2, Supplemental Fig. 2).

788 **Table 2.**

	H-1 (1,3-glucan)	**H-2, 4, and 5 (1,3-)**	**H-3 and 6b (1,3-)**	**H-6a (1,3-)**
LMW	4.52, d, J = 7.8 Hz, 1H	3.20-3.33 m, 3H	~3.5, m, (hidden by H_2O)	3.72, d, J = 11 Hz, 1H
MMW	4.52, d, J = 8.1 Hz, 1H	3.21-3.33 m, 3H	~3.5, m, (hidden by H_2O)	3.72, d, J = 11 Hz, 1H
HMW	4.52, d, J = 7.8 Hz, 1H	3.20-3.32 m, 3H	~3.5, m, (hidden by H_2O)	3.72, d, J = 11 Hz, 1H
Beta 1,3/1,6 Glucan Literature values	4.52, d, J = 8 Hz, 1H	3.25, m, 3H	3.46, m, 2H	3.7, d, J = 11 Hz, 1H

Particulate Glucan

Particulate beta-glucan was prepared from a lyophilized pellet of C. albicans SC5314 yeast. These were boiled in 0.75M NaOH for 15 min, residue was collected, and two additional rounds of the identical treatment were applied. The residue was boiled for 15 min in 2M phosphoric acid, residue was collected and two additional rounds of the identical treatment were applied. The residue was extracted in ethanol with 1% phosphoric acid by boiling for 15 min, residue was collected, and two additional rounds of the identical treatment were applied. The residue was neutralized to pH 7.0, boiled in

809 water for 15 min, residue was collected, and two additional rounds of the identical
810 treatment were applied. The suspension of glucan microparticles was predominantly
811 monodisperse and stored in sterile water at 4C. Depyrogenated glassware and
812 endotoxin free reagents were used in the preparation of glucan particles.

813

814 **Microscopy and Image Analysis**

815 Confocal images were obtained on an Olympus FV1000 laser scanning confocal
816 microscope (Olympus, Center Valley, PA) built around an IX81 inverted microscope.
817 Temperature and CO_2 was controlled at 37°C and 5% respectively. A 10x objective lens
818 (0.40 NA) and a super corrected 60X oil objective lens (1.40 NA), Plan-Apochromat
819 objective lens was used for imaging. Samples were excited with a 473 nm diode laser
820 and a 20 mW, 635 nm diode laser. These lines were reflected to the specimen by a
821 405/473/559/635 multi-edge main dichroic element followed by bandpass emission
822 filters in front of 2 independent High sensitivity GaAsP PMT detector (HSD1/2).
823 Specifically, the emission light passed by the main dichroic was directed to our first
824 detector (HSD1) via SDM560 filter cube and passage through a BA490-540 nm
825 bandpass filter. Our second detector (HSD2) received light from SDM560 filter cube to
826 BA575-675 nm bandpass filter.

827 **Fluo-4 Calcium Imaging**

828 HEK-293 cells expressing Dectin-1A were plated at 40,000 cells in a 35 mm (MatTEK
829 dishes) 24 hours prior to imaging. These cells were loaded with Fluo-4 and Cell Mask
830 Deep Red (CMDR) at equimolar concentrations of 1 μM in 2 mLs of media for one hour

then washed before imaging. Cell Tracker Deep Red was used as a cell cytosolic volume control to account for cytosolic changes from cell contraction that occurs during stimulation. For Syk inhibition, plates were treated with 250 nM of Syk Inhibitor (Calbio chem, #574711) as per the company's specifications. Images were taken at a resolution of 256 x 256 with a dwell time of 2 µs on a 10x objective lens (0.40 NA). A 20 mW, 473 nm diode laser operated at 4% power and CMDR was excited with a 20 mW, 635 nm diode laser operated at 4% power. Fluorescence of Fluo-4 was collected by a cooled GaAsP PMT set to 700V, gain 1X and offset of 0%. Our CMDR was collected through our by a cooled GaAsP PMT detector set to 700V, gain 1X and offset of 0%. 30 frames prior to stimulation were used to set the basal fluorescence of the fluo-4 dye. After stimulation with 100 µl of 10ug/ml of glucan, cells were imaged for 100 frames. To assess changes in intracellular calcium concentration, we measured the ratio of Fluo-4/CMDR intensity in order to correct for any variations in cytoplasmic volume within the confocal section across the field. This ratio was normalized to 1.0 based on mean pre-stimulation values (30 frames) and changes in calcium influx were measured as fold change of this normalized ratio (MFI fold change).

For MMW denaturation experiments, soluble β-glucans were weighed and resuspended in reverse osmosis purified H_2O. In order to denature medium molecular weight glucan, we incubated MMW in DMSO or 1M NaOH. To renature the glucan from DMSO, we placed denatured MMW into Slide-A-Lyzer Dialysis Cassettes (Catalog no. 66203) of a molecular weight cut-off of 2,000 Da and dialyzed against reverse osmosis purified H_2O for 24 hours. To renature glucan from 1M NaOH, the solution was neutralized using 1M HCl.

Protein isolation and immunoblotting

HEK-293 cells stably expressing mEmerald-Dectin-1A were seeded at 5 x 10^5 in 6-well plates 24 hours prior to the experiment. Cells were stimulated with Low, Medium and High molecular weight β-glucan with 1 mg/ml for 5 minutes then lysed. Cells were extracted in 1X lysis buffer (43.9mM HEPES, pH 7.5; 131.7mM NaCl; 1.1% Triton X-100; 8.8% glycerol; 1x protease inhibitor cocktail; 1mM PMSF; 1mM EGTA). Samples were centrifuged at 12,000g for 20 min at 4°C and supernatants transferred to fresh tubes. Protein concentrations were determined by Bradford assay (Bio-Rad Protein Reagent). NuPAGE LDS sample buffer (4X) with NuPAGE Sample Reducing agent (10X) was added to samples (1X final concentration). Total proteins (typically 20-50 µg) were subjected to 4-12% sodium dodecyl sulfate-polyacrylamide gel electrophoresis (SDS-PAGE). Proteins were transferred to Immobilon-FL PVDF transfer membrane (Millipore Sigma) using NuPAGE transfer buffer. Membranes were blocked with bovine serum albumin in Tris-buffered saline-Tween-20 (TBS-T; 20 mM Tris, 137 mM NaCl, 0.1% Tween-20) and incubated with primary antibodies overnight at 4°C. Antibodies purchased from Cell Signaling: Rabbit mAb for p-SYK (Tyr525/526) and β-Actin (13E5), and mouse mAb Syk (4D10) were used according to manufacturer's recommendations (1:1000). HRP-conjugated anti-mouse and anti-rabbit secondary antibodies (Cell Signaling or GE Healthcare) were used at a 1:10,000 dilution. Blots were visualized on a Li-Cor Odyssey FC imaging system and analyzed with Image Studio.

Biolayer interferometry

Advanced Kinetics Biolayer interferometry experiments were conducted using the Personal Assay BLItz System. Anti-human IgG Fc Capture (AHC) Biosensors tips were

initially loaded with Dectin-1A:FC fusion protein (Invivogen, #fc-hdec1a) at 13 ug/ml. Binding kinetics were obtained for LMW, MMW, HMW, MMW (denatured) and MMW (renatured) at 0, 10, 50,100, and 250 nM in triplicate. A global fitting was performed on the curves obtained using the BLItz software.

Congo Red Assay for Glucan Structure

A BioTek EON Multiwell Spectrophotometer was used to analyze Congo Red absorbances. A solution of 8.8 μM Congo Red, 0M-1M NaOH solution (1 M, 0.75 M, 0.5 M, 0.25 M, 0.1 M, 0.075 M, 0.05 M, 0.025 M, 0.001 M, 0 M) and LMW, MMW, or HMW β-glucans at 1 mg/ml were analyzed for the denaturation experiments. For the renaturation experiments, 1mg/ml of β-glucan was denatured at 1M solution then renatured through neutralization with HCl 24 hrs prior to readings. DMSO denaturation conditions involved DMSO in water at 0%, 5% and 10%. For the DMSO renaturation experiments, DMSO was removed by dialysis (see above) prior to spectrophotometer readings. Absorbance readings were taken at 400-700 nm with 1 nm steps. We note that DMSO alone induces a positive shift in the absorbance maximum of Congo Red. This phenomenon mitigates against observation of the full extent of blue shift in Congo Red between untreated glucan and DMSO denatured glucan and tends to reduce the statistical significance of this comparison. Therefore, we present control values for Congo Red with and without DMSO in our data presentation so that the extent of the solvent's effect on the assay may be apparent. All experiments were conducted in technical triplication across three independent experimental replicates.

Fluorescence Lifetime Imaging Microscopy

HEK-293 cells were plated at 25,000 cells in a 35 mm (MatTEK dishes) 48h prior to imaging. Cells were transfected with Emerald-Dectin1A-N-10 and mCherry-Dectin1A-N-10 24 hrs prior to imaging. FLIM-FRET images were obtained using a Leica DMi8 inverted microscope. A Leica Harmonic Compound PL apochromatic CS2 63X water objective with a correction collar (1.2 NA) was used for imaging. A tunable & pulsed White Light Laser (470 - 670 nm) was operated at 80 MHz at 3% laser power using a 488 nm notch filter to excite our sample. A scan speed of 200 and a 256 x 256 resolution was used. Two hybrid detectors collected at photons at (512-540 nm) and (650-700 nm) respectively on the counting mode setting. Temperature was kept at 37 °C using a Tokai Hit Stage Top Incubator for Live Cell Imaging. Lifetime images were collected using a Pico Harp 300 Fluorescence Lifetime Microscopy Time-Correlated Single Photon Counting (TCSPC) system. For our glucan stimulated cells, prior to stimulation 23 frames were collected. 230 frames were taken immediately after stimulated with β-glucans at a concentration of 10 ug/ml. Analysis was conducted on minute time points (1-5 minutes). For yeast contact site imaging studies, 3.5 x10^6 fixed yeast cells were resuspended in 1 ml of PBS. 100 µl of the solution was added to HEK-293 cells in 35 mm dishes 15 minutes prior to imaging. 23 frames were collected per cell. Images were collected at a maximum of 45 minutes after the addition of yeast per plate.

Analysis was conducted on the plasma membrane by masking out internal cellular compartments on the images. For our fungal contact site studies, analysis was conducted on the plasma membrane that was in contact with the fungus and a separate masking for plasma membrane that was not in contact with any yeast. A bi-exponential

fit was performed to the decay curve. For donor only and donor-acceptor on opposite sides of the plasma membrane (negative control) the decay curve indicated a negative amplitude for one of the components, thus indicating a mono-exponential decay was a more accurate representation. Therefore, decay curves from these samples were analyzed using a mono-exponential fit. For cells with donor-acceptor on the cytosolic tail, data was fit to a bi-exponential decay with the first lifetime component being locked at the donor only lifetime of 2.4 ns (τ_D). Lifetime values of the second component (τ_{DA}) of the decay curve were used to calculate FRET efficiency using the equation: $FRET\ Efficiency = \left(1 - \frac{\tau DA}{\tau D}\right) \times 100$. To determine the number of receptors undergoing a FRET process (Donor-acceptor Population), amplitude ratio between the first component (AmpD) and the second component(AmpDA) was calculated according to the following formula: $Donor - Acceptor\ Population = \frac{Amp\ DA}{(AmpD + AmpDA)} \times 100$.

Raster Image Correlation Analysis/Number and Brightness

Protocols on RICS and N&B analysis have been previously described in more depth [55,77]. HEK-293 cells expressing Emerald-Dectin1A-C-10 were plated at 40,000 cells in a 35 mm (MatTEK dishes) 24h prior to imaging. Images were collected at 256 x 256 resolution on a 60× 1.4 NA oil immersion objective lens (Olympus PlanApo/IR) with an optical zoom of 16.4X (0.050 µm pixels). Data was collected using a GaAsP PMT detector operated in photon counting mode. The 473 nm diode laser operated at 0.1% laser power was used in these images. The Point Spread Function (PSF) radial beam waist was estimated using 192 nM EFGP in solution and setting the diffusion coefficient to 90 $\mu m^2/s$. Under these conditions the beam waist was determined to be 0.21 µm.

Immobile features were removed using a 4-frame moving average subtraction. Cells were stimulated with a final concentration of 1 µg/ml of glucan. After stimulation, 200 frames were collected at a pixel dwell time of 4 µs/pixel (line scan of 1.096 ms) with a pinhole size of 100 µm.

Images collected were also used for our Numbers and Brightness analysis, we used 192 nM EGFP in solution and purified mEmerald-GFP protein to set the average brightness of our monomeric protein (Supplemental Fig. 3). Furthermore, the S-factor was calculated using the background image. We divided each brightness distribution by monomeric, dimeric, and oligomeric sections according to previous research [78]. The cursors were scaled quadratically and centered at B values of 1.3, 1.6, and 2.35 for monomers, dimers, and oligomers respectively.

DSTORM analysis

HEK-293 cells, were grown on cleaned and Poly-L-Lysine (0.1 mg/ml) coated coverslips (~$5*10^4$ cells/coverslip) within wells of a six-well plate at 37°C 24hrs prior to the experiment. The cells were then treated with MMW glucan at 1ug/ml for 50 second. The cells were then fixed with paraformaldehyde (PFA; 4%) for 5 minutes at 37 °C followed by three washes of PBS.

Data acquisition was on an Olympus IX-71 microscope equipped with an objective based TIRF illuminator using an oil-immersion objective (PlanApo N, 150×/1.45 NA; Olympus) in an oblique illumination configuration. Sample excitation was done using a 637nm laser (Thorlabs, laser diode HL63133DG), with custom-built collimation optics.

To minimize the drift that occurred during data acquisition, a self-registration algorithm was implemented.

The Dectin-1A nanodomain density was quantified by Super resolution imaging and analyzed using (HSET) as a clustering algorithm in MATLAB. The data for 34 cells for each condition were run through the first pass of HSET to collapse the observations of the blinking fluorophores into single estimates of the true locations of fluorophore [13]. The second HSET pass determined clustering using DBSCAN algorithm [79] which is depend on two parameters (minPts) that is the minimum number of object containing a multi-cluster and the maximum distance between the objects (epsilon). We optimized these parameters for the datasets used in this study at 3 and 27 nm respectively [65].

Collisional FRET Simulation with Monomeric Dectin-1

For this simulation, first a number of particles were generated based on the numbers of fluorophore molecules on the membrane in a specific volume on the real cell. As the experiments have shown that the ratio of donors to acceptors is roughly 50%, in our model 50% of particles were donors while the rest were of acceptors. The absolute number of donor and acceptor molecules was based on experimentally determined Dectin-1A membrane density presented in Fig. 4.

The initial location of each particle was defined by drawing random numbers from a uniform distribution. Throughout the simulation, particle movement was modeled by using a random walk process. The distance each particle moved at each time point was determined by the diffusion coefficient that was experimentally determined and reported in Fig. 4. All particle movements are independent of their type and status.

The simulation space included monomer molecules as donors and acceptors. This simulation space-corresponded to total area of 0.64 μm^2 (equivalent to ~20 pixels membrane area in an experimental FLIM dataset). The total duration of the simulation was 97.6 µs (equivalent to the total experimental data acquisition time for 20 pixels).

Each simulation run included 3904 sequential pulses with each pulse having the equal length of 25 ns (0.1 ns time resolution). At the start of each pulse, 30% donors were selected to act as excited particles. A lifetime value was assigned to each excited particle by generating a random number from an exponential probability density function (τ=2.4 ns; an experimentally determined value of our donor fluorophore). This lifetime value determined how long each excited donor remained excited.

At each time point, after the new location of all particles are calculated (using random walk process), each excited donor neighborhood is checked for acceptors. The neighborhood is defined as a disk with radius of 4-10 nm. In the case where there is an acceptor present in the neighborhood of a specific excited donor, the energy of donor is transferred to the acceptor (see “FRET efficiency” below), which essentially would mean that the donor has decayed. Please note that there are two different phenomena that would result in the decay of excited donors: FRET (as explained in this paragraph) and emission (where the excited donor decay to ground state, according to its characteristic fluorescence lifetime). The total probability of excited state decay is the sum of probabilities from both processes.

Simulation FRET efficiency

With the assumption that the concentration of excited donors is lower than acceptors, concentration, we can consider only one donor molecule. In addition, we assume that orientation factor for dipolar coupling between donor and acceptor is identical for all donor-acceptor pairs because donors and acceptors are considered to be rotating freely. Therefore the FRET efficiency equation is as follows: [80]

$$E = \frac{1}{1 + \sum_{i}^{N} (\frac{R_i}{R_0})^6}$$

The Förster distance (R_0) of the pair of donor and acceptor fluorophores simulated also matches that used for donors and acceptors in FLIM FRET experiments, namely R_0= 5.24 nm [81].The FRET efficiency in this simulation calculates the combination of FRET resulted by acceptors surrounding one excited donor, which are located at some distance from the donor within a specified maximum radial distance, as explained in *Results*.

Software

For the RICS and N&B Data presentation and analysis we used the SimFCS Program (www.lfd.uci.edu). The calcium imaging was analyzed using ImageJ. The FLIM-FRET results were analyzed using Symphotime64 software. The BioLayer interferometry analysis was done using BLItz Pro software. Statistical analysis was performed with GraphPad Prism versions 8.2 (GraphPad Software Inc.). DSTORM analysis and FLIM-FRET modeling was performed using MATLAB using our own algorithm (https://github.com/NeumannLab/FRET-Simulation).

Conflicts of Interest Statement

EUA, AEA and AKN declare that they have no conflicts of interest relevant to this work. We acknowledge that MD and KM are employees of ImmunoResearch, Inc, which provided soluble glucans for this study. MD and KM conducted physicochemical analysis of these glucans and analyzed the results as reported above, but did not determine any other experimental design or data interpretation decisions involved in the work.

Acknowledgements

This research was supported by the University of New Mexico Center for Spatiotemporal Modeling of Cell Signaling (STMC; NIH P50GM085273, AKN) and R01AI116894 (AKN), EUA was supported by fellowships from the STMC and an NIH T32 training grant (NIH T32 AI007538) during the course of this work. We acknowledge the competent technical assistance of Ms. Zinia Pervin in relation to BLI determinations of Dectin-1A/glucan affinity. We acknowledge Diane Lidke for the many helpful discussions on FLIM-FRET and her critical reading and discussion of the manuscript.

References

1. Cleveland AA, Harrison LH, Farley MM, Hollick R, Stein B, Chiller TM, et al. Declining Incidence of Candidemia and the Shifting Epidemiology of Candida Resistance in Two US Metropolitan Areas, 2008–2013: Results from Population-Based Surveillance. Chowdhary A, editor. PLoS One. 2015;10: e0120452. doi:10.1371/journal.pone.0120452

2. Pfaller MA, Diekema DJ. Epidemiology of invasive candidiasis: a persistent public

health problem. Clin Microbiol Rev. 2007;20: 133–63. doi:10.1128/CMR.00029-06

3. Cleveland AA, Farley MM, Harrison LH, Stein B, Hollick R, Lockhart SR, et al. Changes in incidence and antifungal drug resistance in candidemia: results from population-based laboratory surveillance in Atlanta and Baltimore, 2008-2011. Clin Infect Dis. 2012;55: 1352–61. doi:10.1093/cid/cis697

4. Kao AS, Brandt ME, Pruitt WR, Conn LA, Perkins BA, Stephens DS, et al. The Epidemiology of Candidemia in Two United States Cities: Results of a Population-Based Active Surveillance. Clin Infect Dis. 1999;29: 1164–1170. doi:10.1086/313450

5. Hajjeh RA, Sofair AN, Harrison LH, Lyon GM, Arthington-Skaggs BA, Mirza SA, et al. Incidence of bloodstream infections due to Candida species and in vitro susceptibilities of isolates collected from 1998 to 2000 in a population-based active surveillance program. J Clin Microbiol. 2004;42: 1519–27. doi:10.1128/JCM.42.4.1519-1527.2004

6. Antibiotic Resistance Threats in the United States, 2013 | Antibiotic/Antimicrobial Resistance | CDC [Internet]. [cited 24 Jul 2018]. Available: https://www.cdc.gov/drugresistance/threat-report-2013/index.html

7. Chaffin WL. Candida albicans Cell Wall Proteins. Microbiol Mol Biol Rev. 2008;72: 495–544. doi:10.1128/mmbr.00032-07

8. Ruiz-Herrera J, Victoria Elorza M, ValentÃ-n E, Sentandreu R. Molecular organization of the cell wall of *Candida albicans* and its relation to pathogenicity. FEMS Yeast Res. 2006;6: 14–29. doi:10.1111/j.1567-1364.2005.00017.x

1073 9. Gow NAR, Hube B. Importance of the Candida albicans cell wall during
1074 commensalism and infection. Current Opinion in Microbiology. 2012. pp. 406–
1075 412. doi:10.1016/j.mib.2012.04.005

1076 10. Ballou ER, Avelar GM, Childers DS, Mackie J, Bain JM, Wagener J, et al. Lactate
1077 signalling regulates fungal β-glucan masking and immune evasion. Nat Microbiol.
1078 2016;2. doi:10.1038/nmicrobiol.2016.238

1079 11. Sherrington SL, Sorsby E, Mahtey N, Kumwenda P, Lenardon MD, Brown I, et al.
1080 Adaptation of Candida albicans to environmental pH induces cell wall remodelling
1081 and enhances innate immune recognition. PLoS Pathog. 2017;13.
1082 doi:10.1371/journal.ppat.1006403

1083 12. Hopke A, Nicke N, Hidu EE, Degani G, Popolo L, Wheeler RT. Neutrophil Attack
1084 Triggers Extracellular Trap-Dependent Candida Cell Wall Remodeling and Altered
1085 Immune Recognition. PLoS Pathog. 2016;12. doi:10.1371/journal.ppat.1005644

1086 13. Lin J, Wester MJ, Graus MS, Lidke KA, Neumann AK. Nanoscopic cell-wall
1087 architecture of an immunogenic ligand in Candida albicans during antifungal drug
1088 treatment. Mol Biol Cell. 2016;27: 1002–14. doi:10.1091/mbc.E15-06-0355

1089 14. Pappas HC, Sylejmani R, Graus MS, Donabedian PL, Whitten DG, Neumann AK.
1090 Antifungal Properties of Cationic Phenylene Ethynylenes and Their Impact on β-
1091 Glucan Exposure. Antimicrob Agents Chemother. 2016;60: 4519–29.
1092 doi:10.1128/AAC.00317-16

1093 15. Wheeler RT, Kombe D, Agarwala SD, Fink GR. Dynamic, morphotype-specific
1094 Candida albicans β-glucan exposure during infection and drug treatment. PLoS

Pathog. 2008;4. doi:10.1371/journal.ppat.1000227

16. Wheeler RT, Fink GR. A drug-sensitive genetic network masks fungi from the immune system. PLoS Pathog. 2006;2: 328–339. doi:10.1371/journal.ppat.0020035

17. Sletmoen M, Stokke BT. Higher order structure of (1,3)-β-D-glucans and its influence on their biological activities and complexation abilities. Biopolymers. 2008;89: 310–321. doi:10.1002/bip.20920

18. Young SH, Dong WJ, Jacobs RR. Observation of a partially opened triple-helix conformation in 1→3-β- glucan by fluorescence resonance energy transfer spectroscopy. J Biol Chem. 2000;275: 11874–11879. doi:10.1074/jbc.275.16.11874

19. Chuah CT, Sarko A, Deslandes Y, Marchessault RH. Triple-Helical Crystalline Structure of Curdlan and Paramylon Hydrates1 [Internet]. Macromolecules. 1983. Available: https://pubs.acs.org/sharingguidelines

20. Yoshioka Y, Uehara N, Saitô H. Conformation-dependent change in antitumor activity of linear and branched (1----3)-beta-D-glucans on the basis of conformational elucidation by carbon-13 nuclear magnetic resonance spectroscopy. Chem Pharm Bull (Tokyo). 1992;40: 1221–6. doi:10.1248/cpb.40.1221

21. Okobira T, Miyoshi K, Uezu K, Sakurai K, Shinkai S. Molecular dynamics studies of side chain effect on the β-1,3-D-glucan triple helix in aqueous solution. Biomacromolecules. 2008;9: 783–788. doi:10.1021/bm700511d

22. Chihara G, Hamuro J, Maeda Y, Arai Y, Fukuoka F. Fractionation and purification of the polysaccharides with marked antitumor activity, especially lentinan, from Lentinus edodes (Berk.) Sing. (an edible mushroom). Cancer Res. 1970;30: 2776–81. Available: http://www.ncbi.nlm.nih.gov/pubmed/5530561

23. Zhou L, Zhang Q, Zhang Y, Liu J, Cao Y. The shiitake mushroom-derived immuno-stimulant lentinan protects against murine malaria blood-stage infection by evoking adaptive immune-responses. Int Immunopharmacol. 2009;9: 455–62. doi:10.1016/j.intimp.2009.01.010

24. Brown GD, Gordon S. Fungal β-Glucans and Mammalian Immunity. Immunity. 2003;19: 311–315. doi:10.1016/S1074-7613(03)00233-4

25. Novak M, Vetvicka V.) β-Glucans, History, and the Present: Immunomodulatory Aspects and Mechanisms of Action. J Immunotoxicol. 2008;5: 47–57. doi:10.1080/15476910802019045

26. Kim HS, Hong JT, Kim Y, Han S-B. Stimulatory Effect of β-glucans on Immune Cells. Immune Netw. 2011;11: 191. doi:10.4110/in.2011.11.4.191

27. Mueller A, Raptis J, Rice PJ, Kalbfleisch JH, Stout RD, Ensley HE, et al. The influence of glucan polymer structure and solution conformation on binding to (1-->3)-beta-D-glucan receptors in a human monocyte-like cell line. Glycobiology. 2000;10: 339–46. Available: http://www.ncbi.nlm.nih.gov/pubmed/10764821

28. Zhang L, Li X, Xu X, Zeng F. Correlation between antitumor activity, molecular weight, and conformation of lentinan. Carbohydr Res. 2005;340: 1515–21. doi:10.1016/j.carres.2005.02.032

1139 29. Elder MJ, Webster SJ, Chee R, Williams DL, Hill Gaston JS, Goodall JC. β-
1140 Glucan Size Controls Dectin-1-Mediated Immune Responses in Human Dendritic
1141 Cells by Regulating IL-1β Production. Front Immunol. 2017;8: 791.
1142 doi:10.3389/fimmu.2017.00791

1143 30. Di Luzio NR, Williams DL, McNamee RB, Edwards BF, Kitahama A. Comparative
1144 tumor-inhibitory and anti-bacterial activity of soluble and particulate glucan. Int J
1145 cancer. 1979;24: 773–9. doi:10.1002/ijc.2910240613

1146 31. Tzianabos AO. Polysaccharide immunomodulators as therapeutic agents:
1147 structural aspects and biologic function. Clin Microbiol Rev. 2000;13: 523–33.
1148 doi:10.1128/cmr.13.4.523-533.2000

1149 32. Wang Y, Zhang L, Li Y, Hou X, Zeng F. Correlation of structure to antitumor
1150 activities of five derivatives of a β-glucan from Poria cocos sclerotium. Carbohydr
1151 Res. 2004;339: 2567–2574. doi:10.1016/j.carres.2004.08.003

1152 33. Smith AJ, Graves B, Child R, Rice PJ, Ma Z, Lowman DW, et al.
1153 Immunoregulatory Activity of the Natural Product Laminarin Varies Widely as a
1154 Result of Its Physical Properties. J Immunol. 2018;200: 788–799.
1155 doi:10.4049/jimmunol.1701258

1156 34. Suzuki T, Ohno N, Saito K, Yadomae T. Activation of the complement system by
1157 (1----3)-beta-D-glucans having different degrees of branching and different
1158 ultrastructures. J Pharmacobiodyn. 1992;15: 277–85. Available:
1159 http://www.ncbi.nlm.nih.gov/pubmed/1432567

1160 35. Maeda YY, Watanabe ST, Chihara C, Rokutanda M. Denaturation and

renaturation of a beta-1,6;1,3-glucan, lentinan, associated with expression of T-cell-mediated responses. Cancer Res. 1988;48: 671–5. Available: http://www.ncbi.nlm.nih.gov/pubmed/2446749

36. Yanaki T, Ito W, Tabata K, Kojima T, Norisuye T, Takano N, et al. Correlation between the antitumor activity of a polysaccharide schizophyllan and its triple-helical conformation in dilute aqueous solution. Biophys Chem. 1983;17: 337–342. doi:10.1016/0301-4622(83)80018-0

37. Mueller A, Raptis J, Rice PJ, Kalbfleisch JH, Stout RD, Ensley HE, et al. The influence of glucan polymer structure and solution conformation on binding to (1→3)-β-D-glucan receptors in a human monocyte-like cell line. Glycobiology. 2000;10: 339–346. doi:10.1093/glycob/10.4.339

38. Duggan S, Leonhardt I, Hünniger K, Kurzai O. Host response to *Candida albicans* bloodstream infection and sepsis. Virulence. 2015; 1–11. doi:10.4161/21505594.2014.988096

39. Davis SE, Hopke A, Minkin SC, Montedonico AE, Wheeler RT, Reynolds TB, et al. Masking of β(1-3)-glucan in the cell wall of Candida albicans from detection by innate immune cells depends on phosphatidylserine. Infect Immun. 2014;82: 4405–13. doi:10.1128/IAI.01612-14

40. Gow NAR, Netea MG, Munro CA, Ferwerda G, Bates S, Mora-Montes HM, et al. Immune recognition of Candida albicans beta-glucan by dectin-1. J Infect Dis. 2007;196: 1565–71. doi:10.1086/523110

41. Brown GD, Taylor PR, Reid DM, Willment JA, Williams DL, Martinez-Pomares L,

et al. Dectin-1 is a major β-glucan receptor on macrophages. J Exp Med. 2002;196: 407–412. doi:10.1084/jem.20020470

42. Rice PJ, Adams EL, Ozment-Skelton T, Gonzalez AJ, Goldman MP, Lockhart BE, et al. Oral delivery and gastrointestinal absorption of soluble glucans stimulate increased resistance to infectious challenge. J Pharmacol Exp Ther. 2005;314: 1079–86. doi:10.1124/jpet.105.085415

43. O'Neill SK, Getahun A, Gauld SB, Merrell KT, Tamir I, Smith MJ, et al. Monophosphorylation of CD79a and CD79b ITAM motifs initiates a SHIP-1 phosphatase-mediated inhibitory signaling cascade required for B cell anergy. Immunity. 2011;35: 746–756. doi:10.1016/j.immuni.2011.10.011

44. Tomohiro Kurosaki B, AJohnson S, Pao L, Sada K, HirohelYamamura Il, Cambier JC. Role of the Syk Autophosphorylation Site and SH2 Domains in B Cell Antigen Receptor Signaling. doi:10.1084/jem.182.6.1815

45. Hughes CE, Pollitt AY, Mori J, Eble JA, Tomlinson MG, Hartwig JH, et al. CLEC-2 activates Syk through dimerization. Blood. 2010;115: 2947–55. doi:10.1182/blood-2009-08-237834

46. Bartel Y, Bauer B, Steinle A. Modulation of NK cell function by genetically coupled C-type lectin-like receptor/ligand pairs encoded in the human natural killer gene complex. Front Immunol. 2013;4: 362. doi:10.3389/fimmu.2013.00362

47. Hino S, Kito A, Yokoshima R, Sugino R, Oshima K, Morita T, et al. Discharge of solubilized and Dectin-1-reactive β-glucan from macrophage cells phagocytizing insoluble β-glucan particles: Involvement of reactive oxygen species (ROS)-driven

degradation. Biochem Biophys Res Commun. 2012;421: 329–334. doi:10.1016/j.bbrc.2012.04.009

48. Hong F, Yan J, Baran JT, Allendorf DJ, Hansen RD, Ostroff GR, et al. Mechanism by which orally administered beta-1,3-glucans enhance the tumoricidal activity of antitumor monoclonal antibodies in murine tumor models. J Immunol. 2004;173: 797–806. doi:10.4049/jimmunol.173.2.797

49. Gonzalez JA, Digby JD, Rice PJ, Breuel KF, DePonti WK, Kalbfleisch JH, et al. At low serum glucan concentrations there is an inverse correlation between serum glucan and serum cytokine levels in ICU patients with infections. Int Immunopharmacol. 2004;4: 1107–1115. doi:10.1016/J.INTIMP.2004.05.010

50. Digby J, Kalbfleisch J, Glenn A, Larsen A, Browder W, Williams D. Serum glucan levels are not specific for presence of fungal infections in intensive care unit patients. Clin Diagn Lab Immunol. 2003;10: 882–5. doi:10.1128/cdli.10.5.882-885.2003

51. Lowman DW, Ferguson DA, Williams DL. Structural characterization of (1 0/ 3)-b-D-glucans isolated from blastospore and hyphal forms of Candida albicans. doi:10.1016/S0008-6215(03)00169-1

52. Kogan G, Alföldi J, Masler L. 13C-nmr spectroscopic investigation of two yeast cell wall β-D-glucans. Biopolymers. 1988;27: 1055–1063. doi:10.1002/bip.360270702

53. Nitschke J, Modick H, Busch E, von Rekowski RW, Altenbach H-J, Mölleken H. A new colorimetric method to quantify β-1,3-1,6-glucans in comparison with total β-

1,3-glucans in edible mushrooms. Food Chem. 2011;127: 791–796. doi:10.1016/J.FOODCHEM.2010.12.149

54. Brown CM, Dalal RB, Hebert B, Digman MA, Horwitz AR, Gratton E. Raster image correlation spectroscopy (RICS) for measuring fast protein dynamics and concentrations with a commercial laser scanning confocal microscope. J Microsc. 2008;229: 78–91. doi:10.1111/j.1365-2818.2007.01871.x

55. Digman MA, Stakic M, Gratton E. Raster image correlation spectroscopy and number and brightness analysis. Methods Enzymol. 2013;518: 121–44. doi:10.1016/B978-0-12-388422-0.00006-6

56. Bauer B, Steinle A. HemITAM: A single tyrosine motif that packs a punch. Sci Signal. 2017;10: 1–10. doi:10.1126/scisignal.aan3676

57. Brown GD. Dectin-1: a signalling non-TLR pattern-recognition receptor. Nat Rev Immunol. 2006;6: 33–43. doi:10.1038/nri1745

58. Brown J, O'Callaghan CA, Marshall ASJ, Gilbert RJC, Siebold C, Gordon S, et al. Structure of the fungal beta-glucan-binding immune receptor dectin-1: implications for function. Protein Sci. 2007;16: 1042–52. doi:10.1110/ps.072791207

59. Dulal HP, Adachi Y, Ohno N, Yamaguchi Y. β-Glucan-induced cooperative oligomerization of Dectin-1 C-type lectin-like domain. Glycobiology. 2018;28: 612–623. doi:10.1093/glycob/cwy039

60. Singh DR, Kanvinde P, King C, Pasquale EB, Hristova K. The EphA2 receptor is activated through induction of distinct, ligand-dependent oligomeric structures.

Commun Biol. 2018;1: 15. doi:10.1038/s42003-018-0017-7

61. Digman MA, Dalal R, Horwitz AF, Gratton E. Mapping the number of molecules and brightness in the laser scanning microscope. Biophys J. 2008;94: 2320–32. doi:10.1529/biophysj.107.114645

62. Unruh JR, Gratton E. Analysis of molecular concentration and brightness from fluorescence fluctuation data with an electron multiplied CCD camera. Biophys J. 2008;95: 5385–98. doi:10.1529/biophysj.108.130310

63. Trullo A, Corti V, Arza E, Caiolfa VR, Zamai M. Application limits and data correction in number of molecules and brightness analysis. Microsc Res Tech. 2013;76: 1135–1146. doi:10.1002/jemt.22277

64. Wester MJ, Lin J, Neumann AK. A computational model for regulation of nanoscale glucan exposure in Candida albicans. PLoS One. 2017;12. doi:10.1371/journal.pone.0188599

65. Graus MS, Wester MJ, Lowman DW, Williams DL, Kruppa MD, Martinez CM, et al. Mannan Molecular Substructures Control Nanoscale Glucan Exposure in Candida. Cell Rep. 2018;24: 2432-2442.e5. doi:10.1016/j.celrep.2018.07.088

66. OKAZAKI M, ADACHI Y, OHNO N, YADOMAE T. Structure-Activity Relationship of (1.RAR.3)-.BETA.-D-Glucans in the Induction of Cytokine Production from Macrophages, in Vitro. Biol Pharm Bull. 1995;18: 1320–1327. doi:10.1248/bpb.18.1320

67. Cleary JA, Kelly GE, Husband AJ. The effect of molecular weight and β-1,6-

linkages on priming of macrophage function in mice by (1,3)-β- d -glucan. Immunol Cell Biol. 1999;77: 395–403. doi:10.1046/j.1440-1711.1999.00848.x

68. Itano MS, Graus MS, Pehlke C, Wester MJ, Liu P, Lidke KA, et al. Super-resolution imaging of C-type lectin spatial rearrangement within the dendritic cell plasma membrane at fungal microbe contact sites. Front Phys. 2014;2. doi:10.3389/fphy.2014.00046

69. Feinberg H, Guo Y, Mitchell DA, Drickamer K, Weis WI. Extended neck regions stabilize tetramers of the receptors DC-SIGN and DC-SIGNR. J Biol Chem. 2005;280: 1327–35. doi:10.1074/jbc.M409925200

70. Vitale M, Falco M, Castriconi R, Parolini S, Zambello R, Semenzato G, et al. Identification of NKp80, a novel triggering molecule expressed by human NK cells. Eur J Immunol. 2001;31: 233–242. doi:10.1002/1521-4141(200101)31:1<233::AID-IMMU233>3.0.CO;2-4

71. Hanč P, Schulz O, Fischbach H, Martin SR, Kjær S, Reis e Sousa C. A pH- and ionic strength-dependent conformational change in the neck region regulates DNGR-1 function in dendritic cells. EMBO J. 2016;35: 2484–2497. doi:10.15252/embj.201694695

72. Ariizumi K, Shen GL, Shikano S, Xu S, Ritter R, Kumamoto T, et al. Identification of a novel, dendritic cell-associated molecule, dectin-1, by subtractive cDNA cloning. J Biol Chem. 2000;275: 20157–67. doi:10.1074/jbc.M909512199

73. Goodridge HS, Reyes CN, Becker CA, Katsumoto TR, Ma J, Wolf AJ, et al. Activation of the innate immune receptor Dectin-1 upon formation of a “phagocytic

synapse". Nature. 2011;472: 471–5. doi:10.1038/nature10071

74. Graus MS, Pehlke C, Wester MJ, Davidson LB, Steinberg SL, Neumann AK. A New Tool to Quantify Receptor Recruitment to Cell Contact Sites during Host-Pathogen Interaction. Gabhann F Mac, editor. PLoS Comput Biol. 2014;10: e1003639. doi:10.1371/journal.pcbi.1003639

75. Needs PW, Selvendran RR. Avoiding oxidative degradation during sodium hydroxide/methyl iodide-mediated carbohydrate methylation in dimethyl sulfoxide. Carbohydr Res. 1993;245: 1–10. doi:10.1016/0008-6215(93)80055-J

76. Kim YT, Kim EH, Cheong C, Williams DL, Kim CW, Lim ST. Structural characterization of β-D-(1 → 3, 1 → 6)-linked glucans using NMR spectroscopy. Carbohydr Res. 2000;328: 331–341. doi:10.1016/S0008-6215(00)00105-1

77. Youker RT, Teng H. Measuring protein dynamics in live cells: protocols and practical considerations for fluorescence fluctuation microscopy. J Biomed Opt. 2014;19: 090801. doi:10.1117/1.jbo.19.9.090801

78. Planes N, Digman MA, Vanderheyden PPML, Gratton E, Caballero-George C. Number and brightness analysis to study spatio-temporal distribution of the angiotensin II AT1 and the endothelin-1 ETA receptors: Influence of ligand binding. Biochim Biophys Acta - Gen Subj. 2019;1863: 917–924. doi:10.1016/J.BBAGEN.2019.03.004

79. Ester M, Ester M, Kriegel H-P, Sander J, Xu X. A density-based algorithm for discovering clusters in large spatial databases with noise. 1996; 226--231. Available: http://citeseer.ist.psu.edu/viewdoc/summary?doi=10.1.1.121.9220

80. Wolber PK, Hudson BS. An analytic solution to the Förster energy transfer problem in two dimensions. Biophys J. 1979;28: 197–210. doi:10.1016/S0006-3495(79)85171-1

81. Akrap N, Seidel T, Barisas BG. Förster distances for fluorescence resonant energy transfer between mCherry and other visible fluorescent proteins. Anal Biochem. 2010;402: 105–106. doi:10.1016/J.AB.2010.03.026

Supplemental Materials

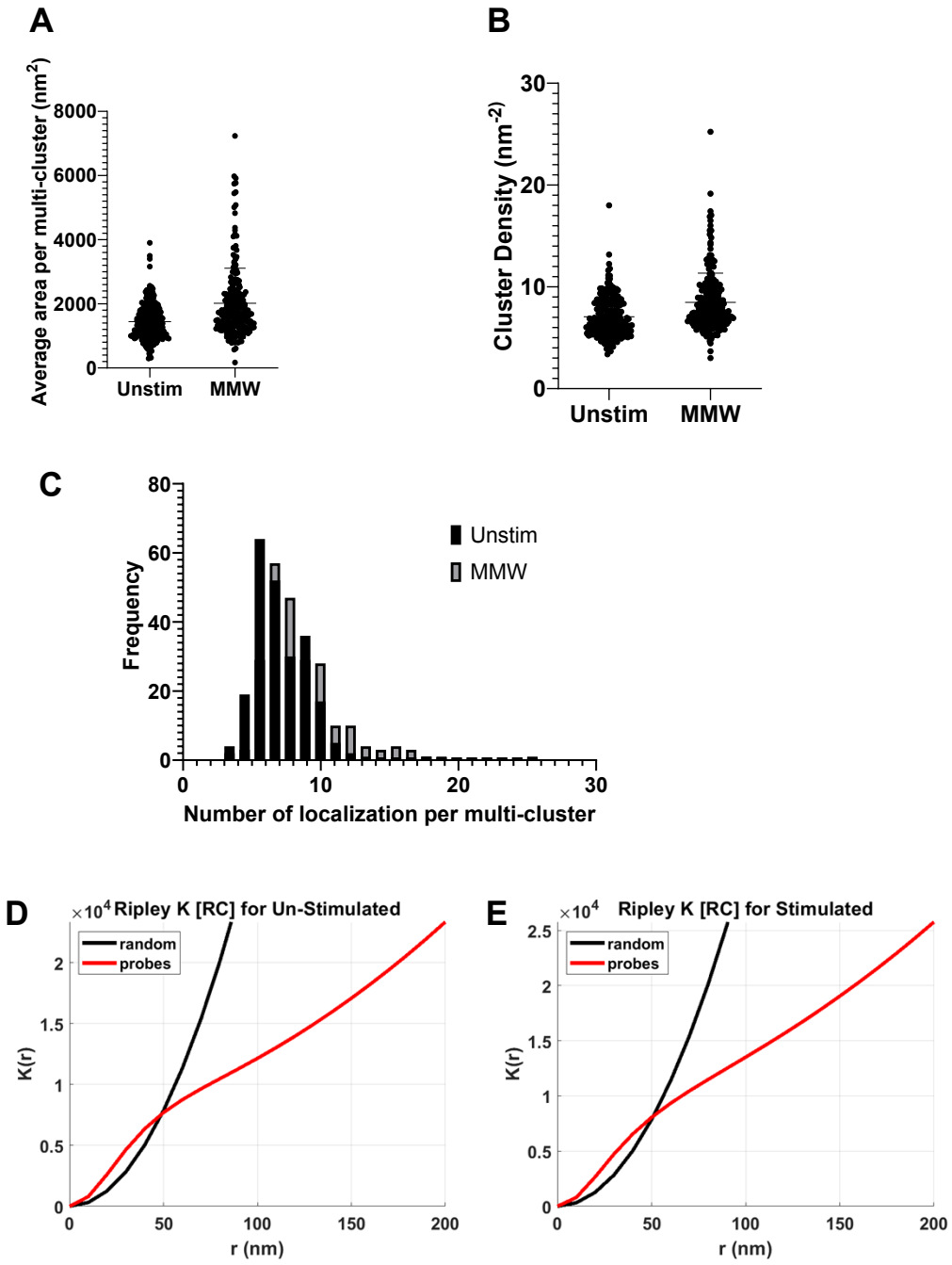

1326

1327 **Supplemental Figure 1: DSTORM Clustering Analysis**

1328 (A) Average area of multi-cluster in dSTORM analysis of HEK-293 cells expressing Dectin-1A

1329 unstimulated or stimulated with MMW. (B) Cluster density of DSTORM analysis of HEK-293 cells

1330 expressing Dectin-1A unstimulated or stimulated with MMW. (C) Histogram analysis of the number of

localizations of HEK-293 cells expressing Dectin-1A unstimulated or stimulated with MMW. (D) Spatial point pattern analysis with Ripley's K function of HEK-293 cells expressing Dectin-1A unstimulated or stimulated with (E) MMW. Data shown as mean ± SD (n = 34)

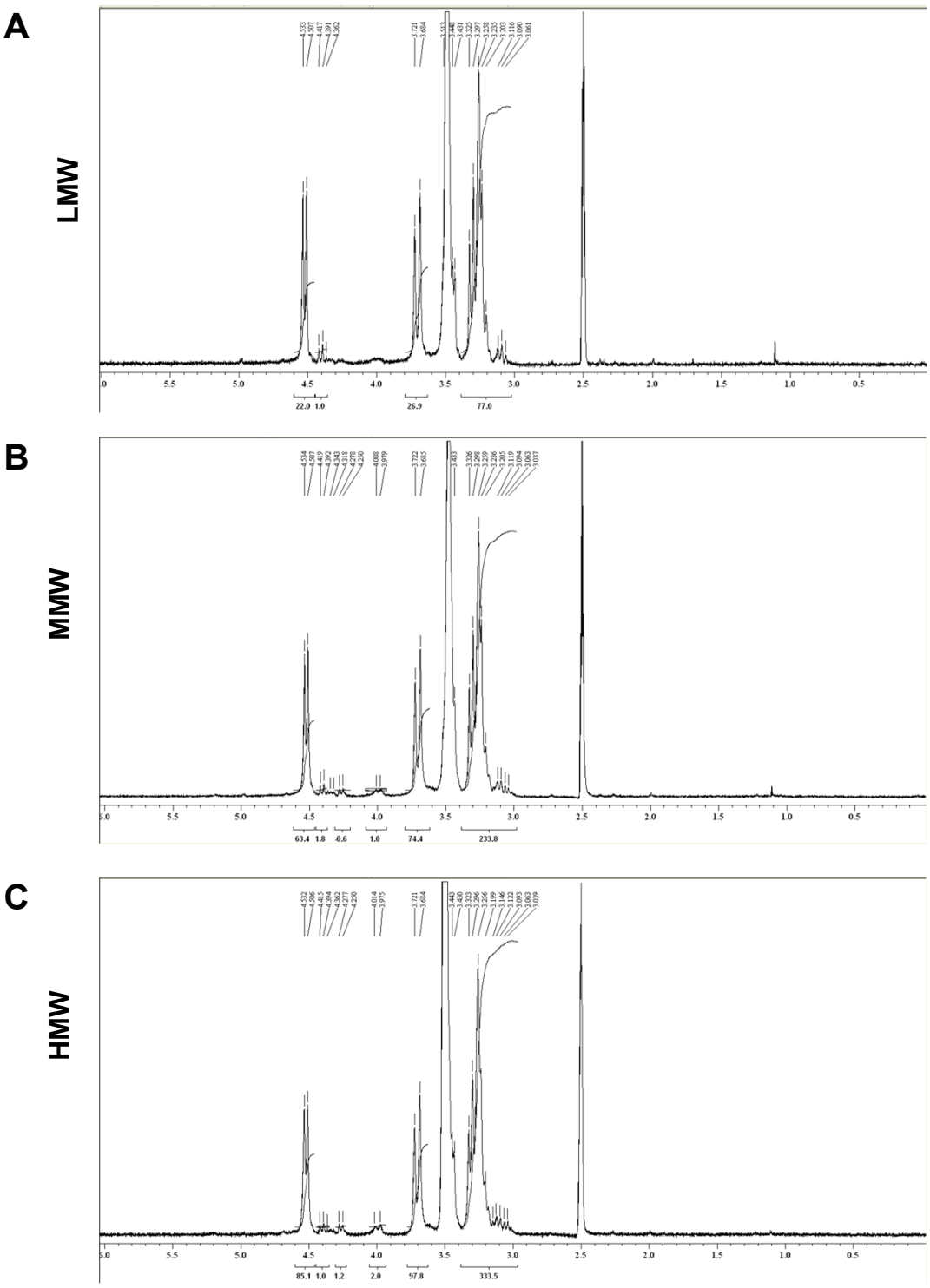

Supplemental Figure 2: ^{1}HNMR Spectrum

(A) ^{1}HNMR spectrum of LMW, (B) MMW, and (C) HMW.

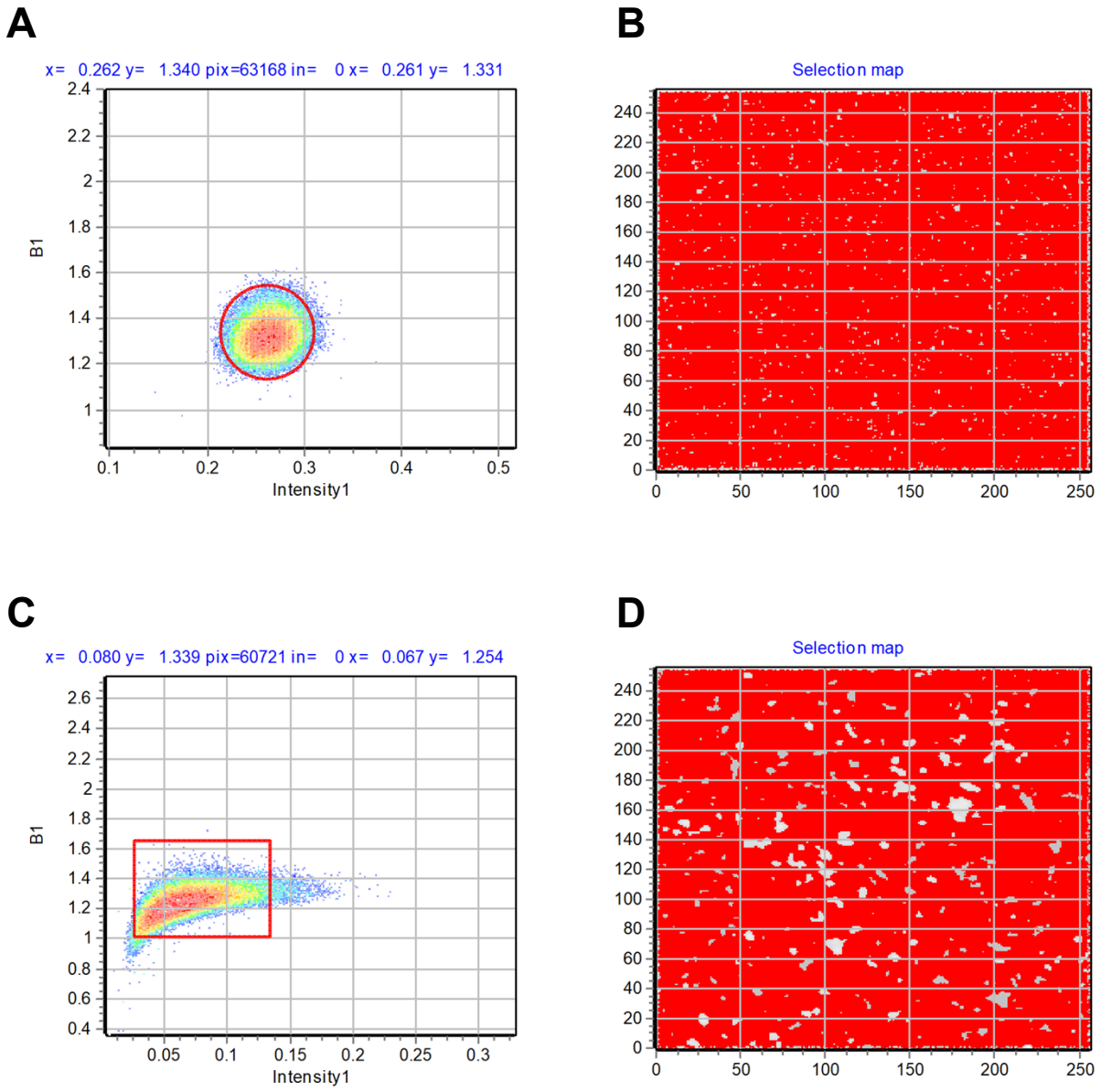

Supplemental Figure 3: Numbers and brightness analysis calibration

(A) Brightness vs intensity 2D histogram of purified EGFP or mEmerald-Dectin-1A (C) with the selected pixels that contribute to the monomers (red) in the image. (B) Representative selection map of purified EGFP or mEmerald-Dectin-1A (D) in which the fluorescent protein populations are defined by colored cursors selected in the Brightness vs intensity histogram.

1345

1346 **Supplemental Table 1.**

Table of Values

	LMW	MMW	HMW
Max Calcium Amplitude	1.2	2.5	1.8

	LMW	MMW	HMW	MMW Denatured	MMW Renatured
Kd (nM)	1.93	1.62	0.43	1.02	1.22

	LMW		MMW		HMW		MMW Denatured	
Min	FRET Efficiency %	Donor-Acceptor %	FRET Efficiency %	Donor-Acceptor %	FRET Efficiency %	Donor-Acceptor %	FRET Efficiency %	Donor-Acceptor %
0	83.3	17.7	76.5	15.3	86.1	14.5	87.5	15.9
1	79.1	17.1	77.0	22.8	80.1	19.5	86.7	15.8
2	79.1	17.9	74.3	22.1	78.9	19.8	86.2	15.1
3	78.5	18.1	77.1	23.7	78.9	21.7	86.3	15.2
4	78.2	19.5	72.1	25.7	79.5	22.5	84.1	16.1
5	77.9	18.8	71.9	28.2	79.5	23.7	84.5	14.1

	N&B			RICS	
	Monomers %	Dimers %	Oligomers %	Diffusion Coefficient ($\mu m^2/s$)	Number of Receptors/μm^2
Unstimulated	74.0	21.4	4.6	1.12	4608
LMW	69.5	20.6	9.9	0.90	3920
MMW	27.5	52.5	20.0	0.37	1768
HMW	37.5	48.7	13.8	0.37	1942

	Singlet Cluster Density (nm^{-2})	Multiple Cluster Density (nm^{-2})	Density of Localizations (nm^{-2})	Average Area per cluster(nm^2)
Unstimulated	0.74	0.59	7.06	1444
MMW	0.77	0.66	8.47	2016

	FRET Efficiency %	Donor- Acceptor %
Cell Membrane	81.8	15.7
SC5314	84.8	15.9
TRL035	78.8	25.1
Glucan Particle	78.8	29.6

1347